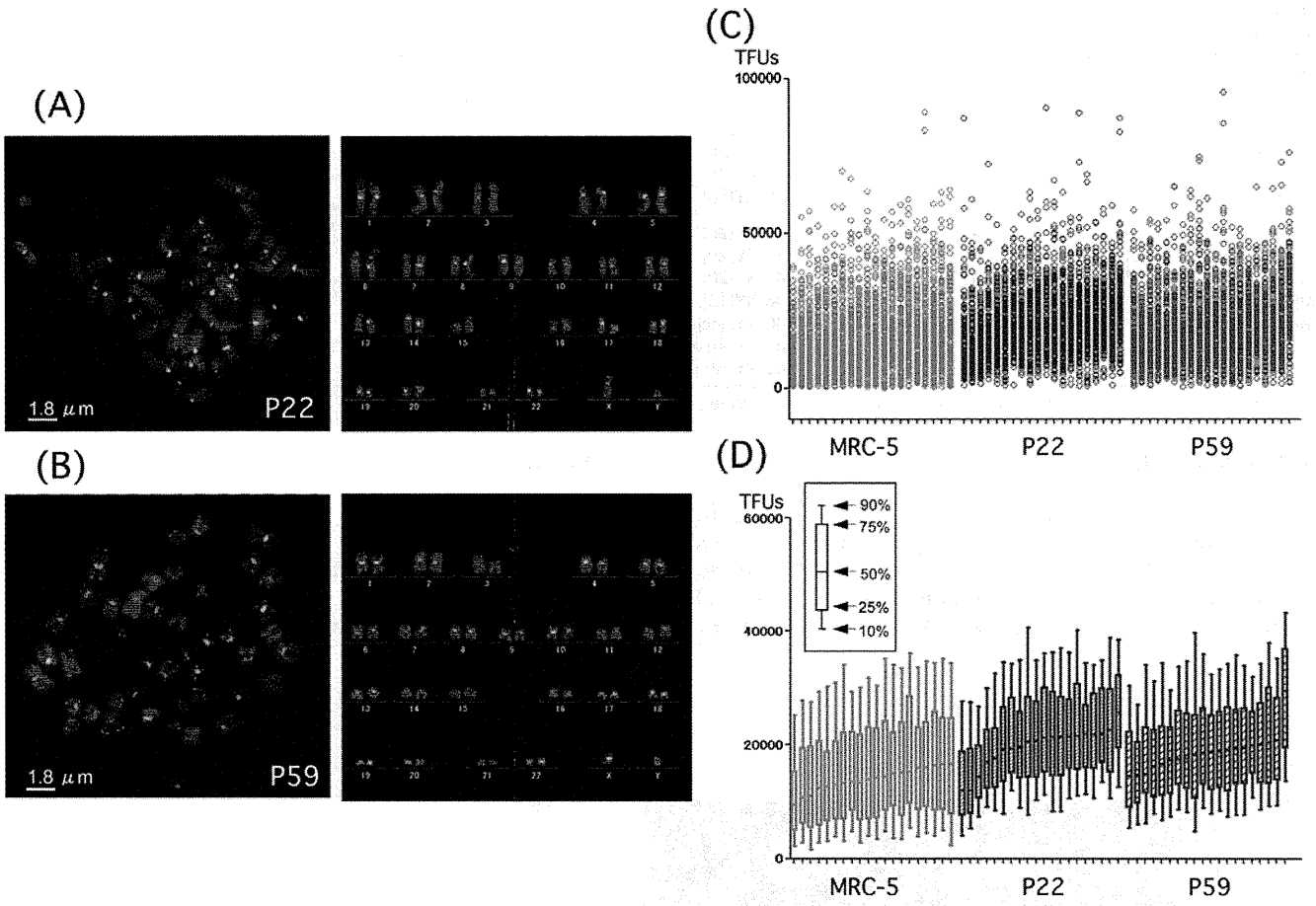

Fig. 2. Karyotype analysis and telomere length measured by Q-FISH and image analyses of MRC-5 iPSCs-16 at passages 22 (A) and 59 (B), and telomere fluorescence units (TFUs, C and D) of the p- and q-arms of all the constituent chromosomes. No chromosomal instability was found. Twenty metaphase spreads of MRC-5 iPSCs-16 at passages 22 and 59 (A, 22P and B, 59P) were examined. Cy3, FITC, and DAPI images were observed after assignment of pseudo-colors (blue for DAPI, red for Cy3 and green for FITC). Labeling with Cy3 and FITC demonstrated the telomere and centromere, respectively. The chromosome preparations were counterstained with DAPI. The telomere fluorescence units (TFUs) of the p- and q-arms of all the chromosomes in the spread were measured individually. The median telomere lengths of 20 metaphase spreads in MRC-5 and MRC-5 iPSCs-16 (passages 22 and 59) are shown as scatter plots for all analyzed data (C) and as box plots (D).

and MRC-5 iPSCs-40 (Nishino et al., 2010, 2011; Cui et al., 2007, 2011). Cy3, FITC, and DAPI images were observed after assignment of pseudo-colors (red for Cy3, green for FITC and blue for DAPI). Twenty metaphase spreads from the parental cells (Fig. 1A), hAM933 iPSCs-2 (passage 25) (Fig. 1B) and hAM933 iPSCs-3 (passage 27) (Fig. 1C), and MRC-5 iPSCs-16 (passages 22 and 59) (Fig. 2A and B) demonstrated no chromosomal instability. None of the 20 parental cell lines, hAM933 iPSCs-2, hAM933 iPSCs-3, or MRC-5 iPSCs-16 (passages 22 and 59) tested showed any abnormality of chromosome number, including X trisomy ($n=1$). However, of the 20 MRC-5 iPSCs-40 (passage 21) cells tested, 19 (95.0%) exhibited normal diploidy and 1 (5.0%) showed chromosomal instability. Of the 20 MRC-5 iPSCs-40 (passage 62) cells tested, all contained abnormal numbers of chromosomes including X ($n=2$) and 12 ($n=8$) trisomies (Fig. 3A and B, Table 1).

4.2. Telomere length (TFU)

We measured telomere lengths in parental cells (hAM933 and MRC-5), two iPSCs (hAM933 iPSCs-2, hAM933 iPSCs-3) derived from different colonies originating from hAM933, and two iPSCs (MRC-5 iPSCs-16 and MRC-5 iPSCs-40) cloned from the same iPSC (MRC-5 iPSCs) at different numbers of passages (MRC-5 iPSCs-16; passages 22 and 59; MRC-5 iPSCs-40; passages 21 and 62) (Table 1).

The median telomere lengths of 20 metaphase spreads in the parental cells, hAM933 iPSCs-2 (passages 25) and hAM933 iPSCs-3 (passages 27), MRC-5 iPSCs-16 (passages 22 and 59), and MRC-5 iPSCs-40 (passages 21 and 62) are shown in Figs. 1D, E, 2C, D, and 3C, D. Scatter plots for all analyzed data are indicated in Figs. 1D, 2C and 3C. The data are summarized as box plots in Figs. 1E, 2D and 3D. Each of the metaphase spreads examined showed marked heterogeneity.

Mean values of the median telomere length in 20 metaphase spreads of parental cells (hAM933 and MRC-5) and all iPSCs are shown in Table 1 and Fig. 4. Mean values for 20 metaphase spreads of the parental cells had a smaller standard deviation than those of iPSCs overall. The established iPSCs, hAM933 iPSCs-2 and hAM933 iPSCs-3, had significantly longer telomeres than hAM933 ($p<0.001$, 1.67 and 1.39), although the telomere extension rate varied quite significantly among the clones ($p<0.001$, 1.67 *versus* 1.39). This observation showed that telomere lengths in an individual iPSC have marked heterogeneity.

The ratios of the mean telomere lengths for medians of 20 metaphase spreads in MRC-5, MRC-5 iPSCs-16 and MRC-5 iPSCs-40, between early and late passages, are shown in Table 1. MRC-5 iPSCs-16 showed no telomere elongation ($p=0.322$, 1.40 and 1.33) as the number of passages increased (22 and 59), whereas MRC-5 iPSCs-40 showed telomere shortening ($p<0.001$, 1.79 and 1.21) as the number of passages increased (21 and 62). The minimum

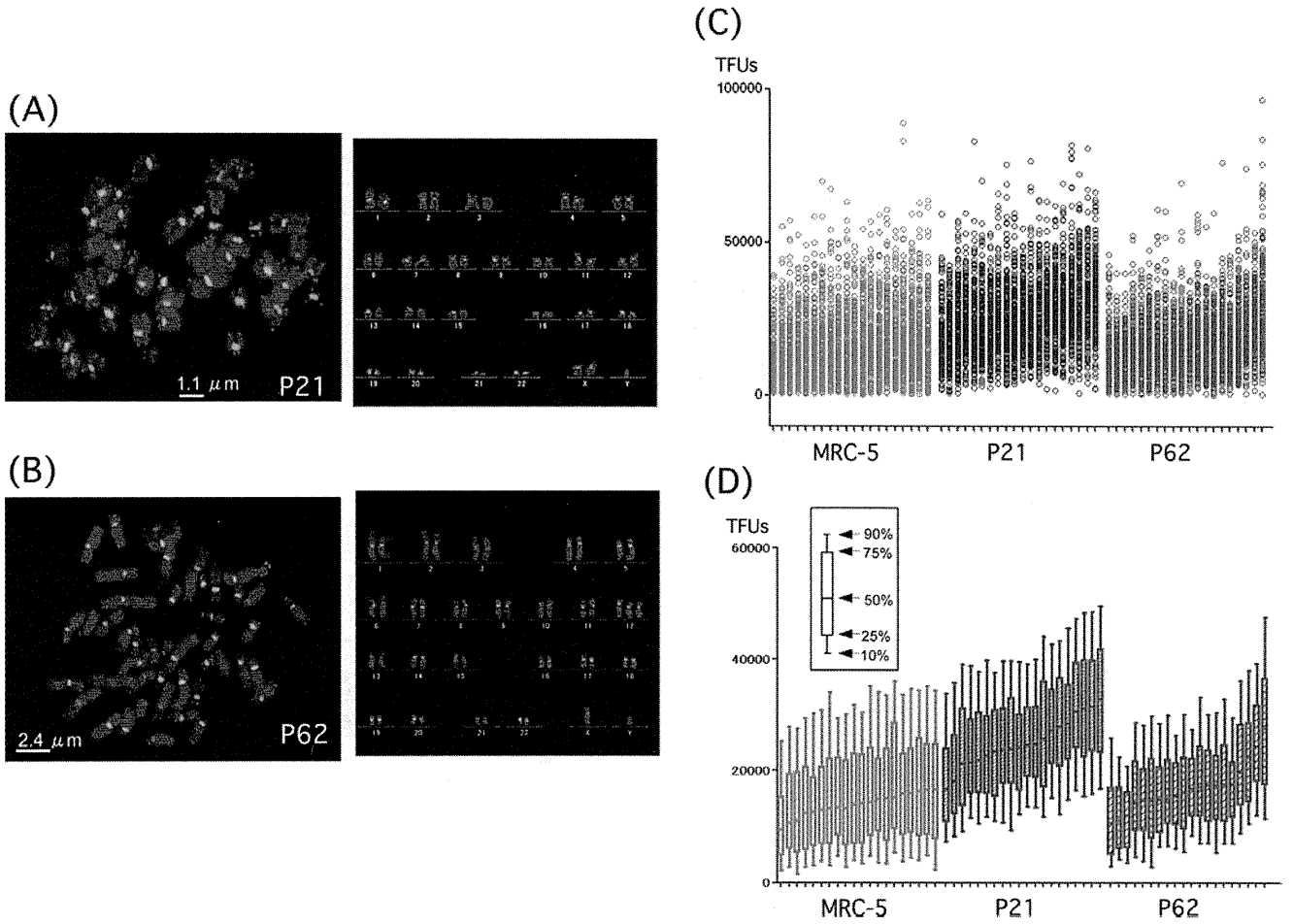

Fig. 3. Karyotype analysis and telomere length measured by Q-FISH and image analyses of MRC-5 iPSCs-40 at passages 21 (A) and 62 (B), and telomere fluorescence units (TFUs, C and D) of the p- and q-arms of all the constituent chromosomes. One (5%) of 20 metaphase spreads showed chromosomal abnormalities including X trisomy at an early stage (A, passages 21) and all 20 showed abnormalities including X and 12 trisomies at the late stage (B, passage 62). Twenty metaphase spreads from MRC-5 iPSCs-40 (21P and 62P; passages 21 and 62) were examined. Cy3, FITC, and DAPI images were observed after assignment of pseudo-colors (blue for DAPI, red for Cy3 and green for FITC). Labeling with Cy3 and FITC demonstrated the telomere and centromere, respectively. The chromosome preparations were counterstained with DAPI. The telomere fluorescence intensities of the p- and q-arms of all the chromosomes in the spread were measured individually. The median telomere lengths of 20 metaphase spreads in MRC-5 and MRC-5 iPSCs-40 (passages 21 and 62) are shown as scatter plots for all analyzed data (C) and as box plots (D).

TFU of MRC-5 iPSC-40 (passage 62, TFU; 371) was smaller than that of MRC-5 (TFU; 380). These results indicated that MRC-5 iPSC-40 with telomere shortening would be susceptible to an abnormal karyotype.

5. Discussion

The initial reports by Yamanaka and others on transcriptional factors directing the reprogramming of somatic cells to a pluripotent state indicated that this event is accompanied by telomerase activation and telomere length extension (Park et al., 2008; Takahashi and Yamanaka, 2006; Takahashi et al., 2007). Activation of telomerase is induced upon establishment of iPSCs, and is dependent on the parental cells of origin. In the present study, the telomeres of parental cells were elongated upon establishment of iPSCs, but the telomere extension rate differed among the clones. These results suggest that establishment of iPSCs induces telomerase activation to various degrees depending on the cell of origin. For telomerase activation, the transcriptional regions of the hTERT need to be switched on, and this process is dependent on the epigenetic information in each individual iPSC. Establishment of iPSCs requires a process of epigenetic reprogramming (Reik, 2007). Epigenetic information is present in the form of DNA methylation, and culture of iPSCs under various conditions can result in stochastic *de novo* methylation (Nishino et al., 2010, 2011). Telomeres become elongated upon establishment of iPSCs, which also acquire telomerase activity and epigenetic changes.

iPSCs are heterogeneous, and also individual iPSCs show a wide range of telomerase expression and telomere length (Wang et al., 2012). Here we found that the iPSCs without telomere shortening showed no significant chromosomal instability as the number of passages increased, whereas the iPSCs with telomere shortening showed significant chromosomal instability with increasing passages. Telomere length represents the potential replicative capacity of a cell, and there is a correlation between the frequency of fusions and telomere length in senescent human cells (Counter et al., 1992; Pereira-Smith and Smith, 1988). Fusions occur between the arms of chromosomes whose telomeres are significantly shorter than average (Aida et al., 2010, 2012; Takubo et al., 2010). We have already developed a method based on estimation of the individual telomere lengths of chromosomal arms of individual cells of different types within independent clones, which exploits the linear correlation between TFUs obtained by Q-FISH and telomere length obtained by Southern blotting (Takubo et al., 2010). Several studies have tried to estimate telomere lengths using tissue sections subjected to Q-FISH (Aida et al., 2008, 2010, 2012; Takubo et al., 2010), and these demonstrated that telomere shortening was associated with an increased incidence of chromosome instability.

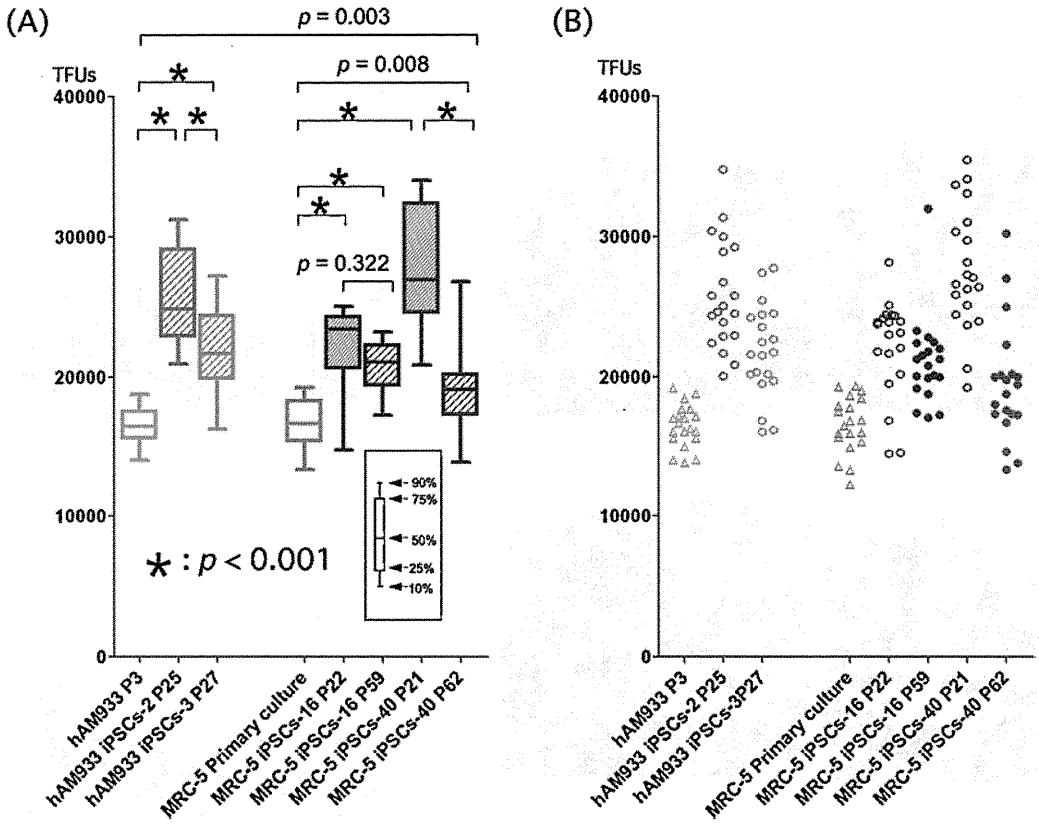

Fig. 4. Mean values of the median telomere length for 20 metaphase spreads in the parental cells (hAM933) and all iPSCs. Box plots (A) and scatter plots for all analyzed data (B). Mean values of 20 metaphase spreads of the parent cells had a smaller S.D. than those of the iPSCs overall. The telomeres of hAM933 iPSCs-2 and hAM933 iPSCs-3 were significantly longer than those of hAM933 ($p < 0.001$, 1.67 and 1.39), although the telomere extension rate varied quite significantly among the clones ($p < 0.001$, 1.67 *versus* 1.39). MRC-5 iPSCs-16 showed no telomere shortening as the number of passages increased (22 and 59) ($p = 0.322$, 1.40 and 1.33), whereas MRC-5 iPSCs-40 showed telomere shortening as the number of passages increased (21 and 62) ($p < 0.001$, 1.79 and 1.21). The mean telomere lengths of the median telomere lengths for 20 metaphase spreads in the parent cells and all iPSCs are shown as scatter plots for box plots (A) and all analyzed data (B).

These studies demonstrating excessive telomere shortening in the background epithelium have also suggested that this is an initial feature in the process of cancerization (Aida et al., 2010, 2012; Takubo et al., 2010). Our present study indicated that although established iPSCs maintain telomerase activity, chromosomal instability can be induced by telomere shortening. This suggests that iPSCs showing telomere shortening associated with an increased number of passages or chromosomal instability should probably not be chosen for experimental or therapeutic purposes.

The establishment of iPSCs appeared to be associated with telomere elongation and activation of telomerase. The heterogeneity of telomerase expression in iPSCs suggests that cellular senescence could be controlled by the chromosomes of individual cells, and that short telomeres arising as a result of limiting levels of telomerase predispose chromosomes to instability. Long-term culture of iPSCs would induce random methylation and convergence, and telomere activation might be influenced by epigenetic regions of hTERT transcription. iPSCs comprise convergent cells in which stochastic methylation, selection and fixation would be dependent on environment conditions. It has been proposed that cell therapy using iPS cells for a variety of patients with genetically complex and heterogeneous diseases would have both advantages and limitations, although iPSCs with alleles from the patient would provide an abundant material for clarifying the molecular mechanisms of disease in a variety of genotypes, thus facilitating the development of tailored therapy (Agarwal and Daley, 2011; Agarwal et al., 2010). If iPSCs are applied for cell therapies in the future, reprogramming techniques will need to consider the expression of specific genes in individual cells. Telomere measurement would also be useful for guaranteeing the quality of iPSCs, and further studies will be necessary to clarify the telomere metabolism of iPSCs in detail.

6. Conclusions

The telomere lengths of iPSC clones, represented as mean values of median telomere fluorescence units, significantly exceeded those of the parental strain, while the telomere extension rates varied significantly between the clones.

iPSCs established from fetal lung fibroblast (MRC-5) did not exhibit telomere shortening and chromosomal instability as the number of passages increased. However, the telomeres of other iPSCs derived from MRC-5 became shorter as the number of passages increased; one (5%) of 20 metaphase spreads showed chromosomal abnormalities including X trisomy at an early stage, and all 20 showed abnormalities including X and 12 trisomies at the late stage.

Conflict of interest statement

The authors have no conflicts of interest to declare in relation to this study.

Acknowledgements

This work was supported by JSPS KAKENHI: 21390109 (K.T.) and 16590300 (K.N.).

References

Agarwal., S., Daley, G.Q., 2011. Telomere dynamics in dyskeratosis congenita: the long and the short of iPS. Cell Res. 21, 1157–1160.

Agarwal, S., Loh, Y.H., McLoughlin, E.M., Huang, J., Park, I.H., Miller, J.D., Huo, H., Okuka, M., Dos Reis, R.M., Loewer, S., Ng, H.H., Keefe, D.L., Goldman, F.D., Klingelhutz, A.J., Liu, L., Daley, G.Q., 2010. Telomere elongation in induced pluripotent stem cells from dyskeratosis congenita patients. Nature 464, 292–296.

Aida, J., Izumiyama-Shimomura, N., Nakamura, K., Ishikawa, N., Poon, S.S., Kammori, M., Sawabe, M., Arai, T., Matsuura, M., Fujiwara, M., Kishimoto, H., Takubo, K., 2008. Basal cells have longest telomeres measured by tissue Q-FISH method in lingual epithelium. Exp. Gerontol. 43, 833–839.

Aida, J., Izumo, T., Shimomura, N., Nakamura, K., Ishikawa, N., Matsuura, M., Poon, S.S., Fujiwara, M., Sawabe, M., Arai, T., Takubo, K., 2010. Telomere lengths in the oral epithelia with and without carcinoma. Eur. J. Cancer 46, 430–438.

Aida, J., Kobayashi, T., Saku, T., Yamaguchi, M., Shimomura, N., Nakamura, K., Ishikawa, N., Maruyama, S., Cheng, J., Poon, S.S., Sawabe, M., Arai, T., Takubo, K., 2012. Short telomeres in an oral precancerous lesion: Q-FISH analysis of leukoplakia. J. Oral Pathol. Med. 41, 372–378.

Apostolou, E., Hochedlinger, K., 2011. Stem cells: iPS cells under attack. Nature 474, 165–166.

Aubert, G., Hills, M., Lansdorp, P.M., 2012. Telomere length measurement-caveats and a critical assessment of the available technologies and tools. Mutat. Res. 730, 59–67.

Blackburn, E.H., 2001. Switching and signaling at the telomere. Cell 106, 661–673.

Counter, C.M., Avilion, A.A., LeFeuvre, C.E., Stewart, N.G., Greider, C.W., Harley, C.B., Bacchetti, S., 1992. Telomere shortening associated with chromosome instability is arrested in immortal cells which express telomerase activity. EMBO J. 11, 1921–1929.

Cui, C.H., Miyoshi, S., Tsuji, H., Makino, H., Kanzaki, S., Kami, D., Terai, M., Suzuki, H., Umezawa, A., 2011. Dystrophin conferral using human endothelium expressing HLA-E in the non-immunosuppressive murine model of Duchenne muscular dystrophy. Hum. Mol. Genet. 20, 235–244.

Cui, C.H., Uyama, T., Miyado, K., Terai, M., Kyo, S., Kiyono, T., Umezawa, A., 2007. Menstrual blood-derived cells confer human dystrophin expression in the murine model of Duchenne muscular dystrophy via cell fusion and myogenic transdifferentiation. Mol. Biol. Cell 18, 1586–1594.

de Lange, T., 2005. Shelterin: the protein complex that shapes and safeguards human telomeres. Genes Dev. 19, 2100–2110.

Liu, Z., Wan, H., Wang, E., Zhao, X., Ding, C., Zhou, S., Li, T., Shuai, L., Feng, C., Yu, Y., Zhou, Q., Beaujean, N., 2012. Induced pluripotent stem-induced cells show better constitutive heterochromatin remodeling and developmental potential after nuclear transfer than their parental cells. Stem Cells Dev. 21, 3001–3009.

Nishino, K., Toyoda, M., Yamazaki-Inoue, M., Fukawatase, Y., Chikazawa, E., Sakaguchi, H., Akutsu, H., Umezawa, A., 2011. DNA methylation dynamics in human induced pluripotent stem cells over time. PLoS Genet. 7, e1002085.

Nishino, K., Toyoda, M., Yamazaki-Inoue, M., Makino, H., Fukawatase, Y., Chikazawa, E., Takahashi, Y., Miyagawa, Y., Okita, H., Kiyokawa, N., Akutsu, H., Umezawa, A., 2010. Defining hypo-methylated regions of stem cell-specific promoters in human iPS cells derived from extra-embryonic amnions and lung fibroblasts. PLoS ONE 5, e13017.

Park, I.H., Zhao, R., West, J.A., Yabuuchi, A., Huo, H., Ince, T.A., Lerou, P.H., Lensch, M.W., Daley, G.Q., 2008. Reprogramming of human somatic cells to pluripotency with defined factors. Nature 451, 141–146.

Pereira-Smith, O.M., Smith, J.R., 1988. Genetic analysis of indefinite division in human cells: identification of four complementation groups. Proc. Natl. Acad. Sci. U.S.A. 85, 6042–6046.

Poon, S.S., Lansdorp, P.M., 2001a. Quantitative fluorescence in situ hybridization (Q-FISH). Curr. Protoc. Cell Biol. (Chapter 18, Unit 18.4).

Poon, S.S., Lansdorp, P.M., 2001b. Measurements of telomere length on individual chromosomes by image cytometry. Methods Cell Biol. 64, 69–96.

Reik, W., 2007. Stability and flexibility of epigenetic gene regulation in mammalian development. Nature 447, 425–432.

Shaffer, L.G., Slovak, M.L., Campbell, L.J., 2009. ISCN 2009. An International System for Human Cytogenetic Nomenclature: Recommendations of the International Standing Committee on Human Cytogenetic Nomenclature. S. Karger Co., Basel.

Suhr, S.T., Chang, E.A., Rodriguez, R.M., Wang, K., Ross, P.J., Beyhan, Z., Murthy, S., Cibelli, J.B., 2009. Telomere dynamics in human cells reprogrammed to pluripotency. PLoS ONE 4, e8124.

Takahashi, K., Tanabe, K., Ohnuki, M., Narita, M., Ichisaka, T., Tomoda, K., Yamanaka, S., 2007. Induction of pluripotent stem cells from adult human fibroblasts by defined factors. Cell 131, 861–872.

Takahashi, K., Yamanaka, S., 2006. Induction of pluripotent stem cells from mouseembryonic and adult fibroblast cultures by defined factors. Cell 126, 663–676.

Takubo, K., Aida, J., Izumiyama, N., Ishikawa, N., Fujiwara, M., Poon, S.S., Kondo, H., Kammori, M., Matsuura, M., Sawabe, M., Arai, T., Baird, D.M., Nakamura, K., 2010. Chromosomal instability and telomere lengths of each chromosomal arm measured by Q-FISH in human fibroblast strains prior to replicative senescence. Mech. Ageing Dev. 131, 614–624.

Vaziri, H., Dragowska, W., Allsopp, R.C., Thomas, T.E., Harley, C.B., Lansdorp, P.M., 1994. Evidence for a mitotic clock in human hematopoietic stem cells: loss of telomeric DNA with age. Proc. Natl. Acad. Sci. U.S.A. 91, 9857–9860.

Wang, F., Yin, Y., Ye, X., Liu, K., Zhu, H., Wang, L., Chiourea, M., Okuka, M., Ji, G., Dan, J., Zuo, B., Li, M., Zhang, Q., Liu, N., Chen, L., Pan, X., Gagos, S., Keefe, D.L., Liu, L., 2012. Molecular insights into the heterogeneity of telomere reprogramming in induced pluripotent stem cells. Cell Res. 22, 757–768.

Kami et al. BMC Biotechnology 2013, 13:102
http://www.biomedcentral.com/1472-6750/13/102

BMC Biotechnology

RESEARCH ARTICLE Open Access

Large-scale cell production of stem cells for clinical application using the automated cell processing machine

Daisuke Kami[1], Keizo Watakabe[2], Mayu Yamazaki-Inoue[3], Kahori Minami[3], Tomoya Kitani[4], Yoko Itakura[5], Masashi Toyoda[5], Takashi Sakurai[2], Akihiro Umezawa[3] and Satoshi Gojo[1*]

Abstract

Background: Cell-based regeneration therapies have great potential for application in new areas in clinical medicine, although some obstacles still remain to be overcome for a wide range of clinical applications. One major impediment is the difficulty in large-scale production of cells of interest with reproducibility. Current protocols of cell therapy require a time-consuming and laborious manual process. To solve this problem, we focused on the robotics of an automated and high-throughput cell culture system. Automated robotic cultivation of stem or progenitor cells in clinical trials has not been reported till date. The system AutoCulture® used in this study can automatically replace the culture medium, centrifuge cells, split cells, and take photographs for morphological assessment. We examined the feasibility of this system in a clinical setting.

Results: We observed similar characteristics by both the culture methods in terms of the growth rate, gene expression profile, cell surface profile by fluorescence-activated cell sorting, surface glycan profile, and genomic DNA stability. These results indicate that AutoCulture® is a feasible method for the cultivation of human cells for regenerative medicine.

Conclusions: An automated cell-processing machine will play important roles in cell therapy and have widespread use from application in multicenter trials to provision of off-the-shelf cell products.

Keywords: Automated cell culture system, Cell transplantation, Stem cells, Clinical trial, Cell processing facility

Background

Degenerative diseases affect increasing numbers of people, particularly in developed countries with aging populations. Despite advancements in medicine, modalities to cure advanced diseases are often not available. Therefore, regenerative therapy may become the standard treatment option in cardiovascular medicine. Recent developments in stem cell biology, including those related to induced pluripotent stem cells (iPSCs) and tissue-derived stem/progenitor cells, are a giant leap toward the goal. Recently, myocardium-derived stem/progenitor cells were isolated by several institutes [1-3]. These cell populations have the potential to repair the diseased heart, and clinical trials are currently ongoing.

In tandem with these developments in stem cell biology and the large number of completed and ongoing clinical trials, attempts have been made to commercialize these therapies [4]. The most prominent therapeutic strategy is cell transplantation. However, harvested cells or tissues are usually limited in quantity and stem cells properties may vary from batch to batch, hindering the reliability for clinical applications. Moreover, current cell therapy protocols are laboratory centered and labor intensive, requiring highly skilled personnel and weeks to months to harvest sufficient quantities of stem/progenitor cells from the isolated tissues. These manual procedures are expensive and can result in high phenotypic and yield variability between different trials and institutions [5].

Strategies to validate advanced medicinal products have been established; however, these "best practices" still depend on the ability of personnel to perform them, such as the cultivation of stem/progenitor cells under strictly

* Correspondence: gojos@koto.kpu-m.ac.jp
[1]Department of Regenerative Medicine, Kyoto Prefectural University of Medicine, 465 Kajii-cho, Kawaramachi-Hirokoji, Kamigyo-ku, Kyoto 602-8566, Japan
Full list of author information is available at the end of the article

controlled conditions [6]. High process reproducibility can be achieved by automation, and several effective automatic cell culture systems have been reported [7-12]. These automated platforms have the potential to provide cost-effective, large-scale expansion of stem/progenitor cells with consistent phenotype for clinical use and improved operational safety [13]. Progress in robot platforms for cell culture has resulted in several prototypes to implement large-scale expansion and harvesting of stem/progenitor cells with yield and phenotypic reproducibility. An automated culture system by "The Automation Partnership Biosystems (TAP Biosystems)" has cultivated human embryonic stem cells and bone marrow-derived cells [14,15]. Kawasaki Heavy Industries (Tokyo, Japan) has created AutoCulture® (Additional file 1), which can automate many manual steps in cell culture, including media exchange, centrifugation of cells, splitting and passaging, and recording of cell morphology (Figure 1A). To the best of our knowledge, no cell products obtained from an automated culture apparatus have actually been transplanted into humans for regenerative therapy.

Our institute recently completed a phase I clinical trial using autologous cardiac stem cells (CSCs) isolated by manual cell culture techniques to treat ischemic cardiomyopathy [16]. The trial is registered in the Japanese government database for clinical trials using human stem cells and ClinicalTrials.gov, which is a world-wide registry and results database for clinical trials involving humans, as AutoLogous Human CArdiac-Derived Stem Cell to Treat Ischemic cArdiomyopathy (ALCADIA; Identifier: NCT00981006). CSCs are manually cultivated by a single experienced investigator for approximately 1 month to minimize variability of the final cell products. To advance this trial from a single-center to a multi-center randomized trial, we evaluated AutoCulture® by comparing the growth rate, morphology, and phenotype of cells cultivated using this method with those of manually cultured CSCs.

Results

Cellular morphology and growth

Calculations based on the net cell number and doubling time obtained in the ALCADIA trial (Additional file 2)

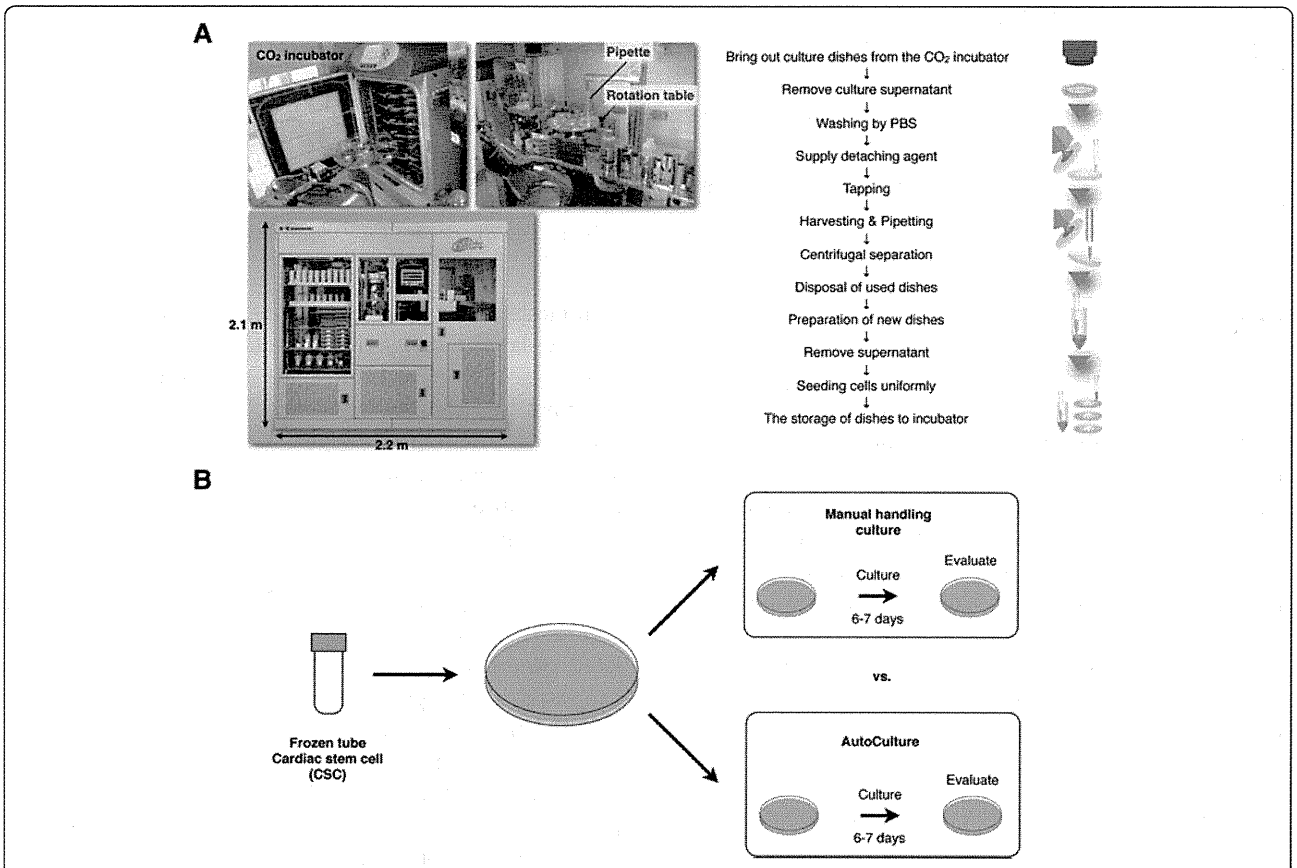

Figure 1 Process maps showing the key steps in human cardiac stem cell culture using manual methods and the AutoCulture® system. **(A)** The automated culture system AutoCulture® by Kawasaki Heavy Industries (left) can automate every step of manual cell culture under current good manufacturing practice (cGMP) grade. **(B)** Schematic representation of the experiment. Human cardiac stem cells (CSCs) were thawed and split into 2 dishes for either manual culture or automated culture using AutoCulture®.

indicated that a culture duration of 2 weeks was sufficient to obtain the appropriate cell number for clinical trial when cells after the second passage (P2) were used as the starting material. Identically seeded culture plates were maintained manually or by automation using AutoCulture® (Figure 1B). The morphology of CSCs cultured using the automated system was similar to that of manually cultured CSCs on day 7 and 14 after seeding (Figure 2A). Under both the conditions, the cells were of similar size, exhibited a low nucleus/cytoplasm ratio, and had a spindle-like shape. In addition, the growth rate was not significantly different, as indicated by cell counts at passage (Figure 2B). Trypan blue staining revealed no significant difference in cell viability between the culture methods. Moreover, both the methods effectively washed out the cells, as indicated by the paucity of adherent cells on discarded culture dishes (data not shown). These results suggest that manual passage was effectively replicated using AutoCulture®.

Gene expression

To investigate the gene expression profiles, RT-PCR analysis was performed according to the shipping criteria for cultivated cells in the current clinical trial (ALCADIA). We examined expression levels of the pluripotency related genes *NANOG*, *OCT4*, *SOX2*, and *REX1* and 2 transcription factor genes involved in cardiomyocyte development, *NKX2.5* and *GATA4* (Figure 2C). The stem cell markers *OCT4*, *REX1*, and *GATA4* were expressed by both cell populations; however, neither *NANOG* nor *NKX2.5* expression was detectable. Moreover, expression levels were not significantly different between the 2 groups on either day 7 or day 14.

Cell surface marker expression profiles

Cell surface markers indicative of CSCs and other phenotypes were detected by fluorescence-activated cell sorting (FACS) (Figure 3A). Under both the culture conditions, the cells were positive for the mesenchymal stem cell (MSC) markers CD29 and CD90 and the vascular endothelial marker CD105 and negative for the hematopoietic lineage marker CD45 and MHC class II. In addition, fluorescent intensities measured by FACS were similar for all positive markers, indicating that equal proportions of cells in both the populations expressed these proteins. Moreover, almost all the cells were CD29 positive, whereas at least 2 populations were distinguished on the basis of CD90 expression. Furthermore, STRO-1, which is expressed by mesenchymal stem cells in the bone marrow, was negative in both the populations. Although the surface expression profiles of CSCs and bone marrow-derived stem cells overlap, STRO-1 expression can discriminate cardiac MSCs from bone marrow-derived MSCs.

Surface glycan expression profile by lectin microarray analysis

Recently, glycan expression profiling has been reported to be an effective cell validation tool to complement phenotype analysis by epigenetic and gene expression analyses

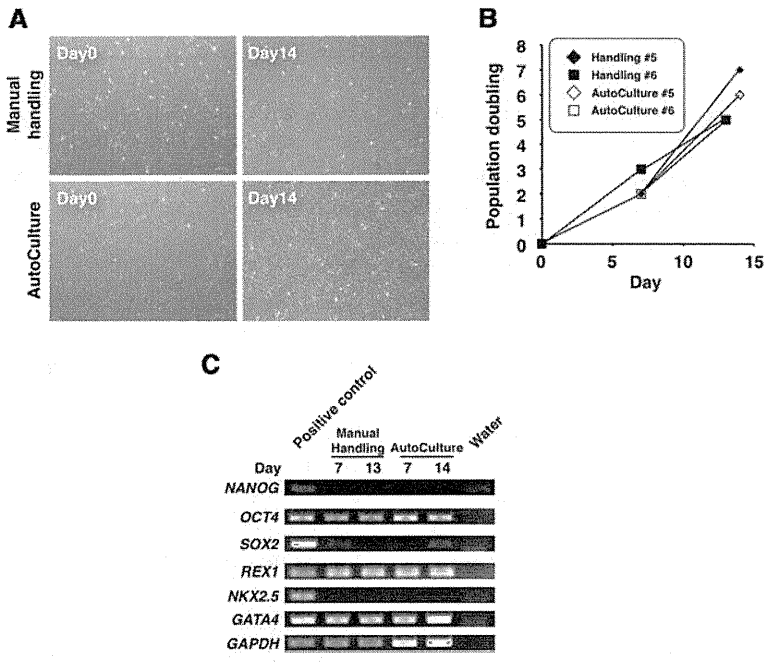

Figure 2 Phenotypic characterizations of CSCs during manual and automated culture. (A) Phase contrast microphotographs of CSCs cultivated either by manual handling (upper panels) or using AutoCulture® (lower panels). **(B)** Growth rates of CSCs under manual or automated culture. **(C)** RT-PCR analysis of genes related to pluripotency and cardiac-specific transcription factors.

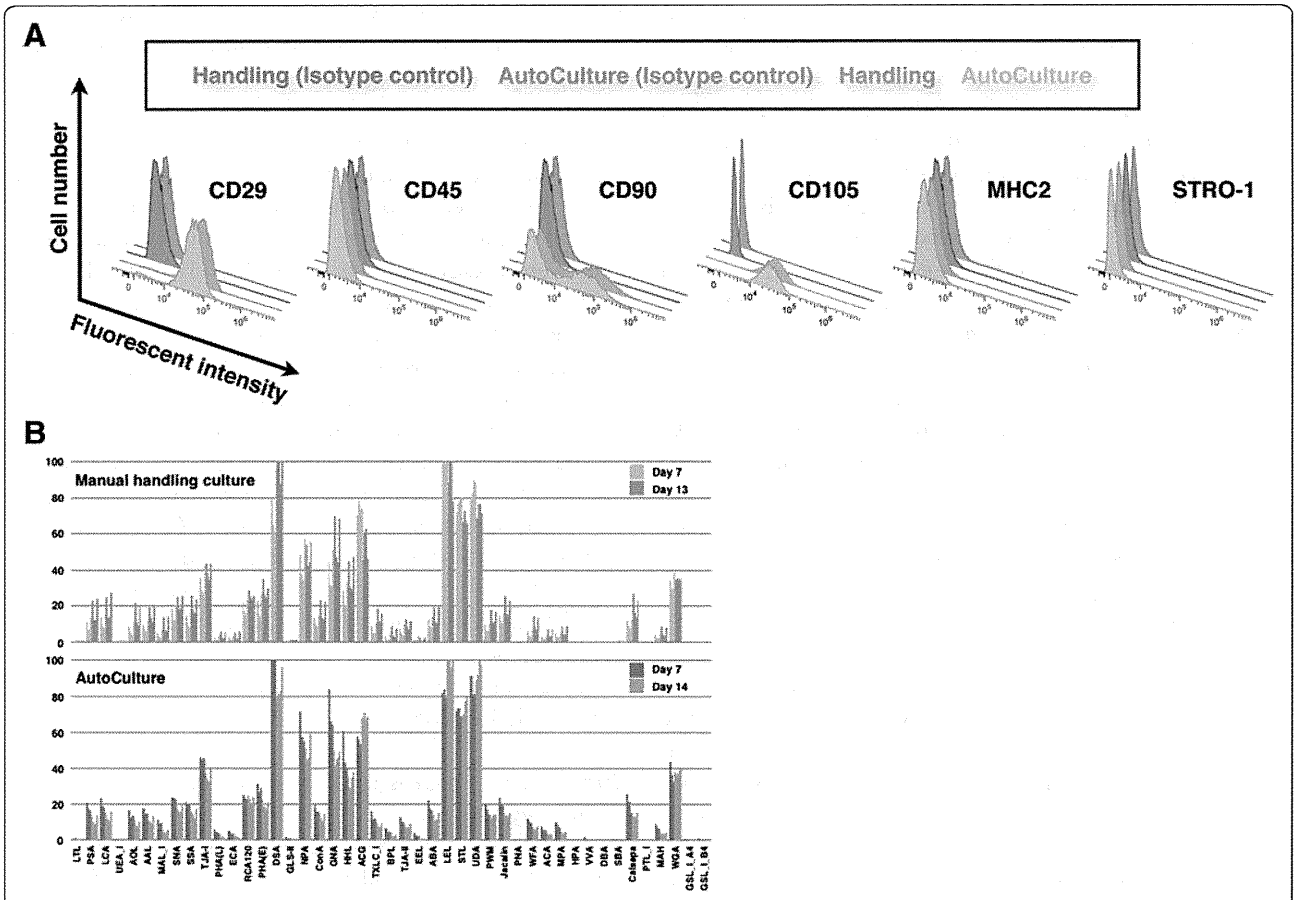

Figure 3 Analysis of cell surface protein and glycan expression in CSCs expanded by manual culture or AutoCulture®. (A) Cells were stained with fluorescence-conjugated primary antibodies and analyzed for surface expression by fluorescence-activated cell sorting. **(B)** Lectin microarray analysis of manual cultures and cells maintained using AutoCulture® on day 7 and day 13/14. The glycan profiles showed little difference between the two culture groups at any time.

[17]. These lectin profiles showed similar patterns, and no significant differences in expression intensities were observed between the 2 culture groups on either day 7 or day 13/14 after seeding (Figure 3B). The washing process used to harvest adherent cells may have profound effects on the cell surface structure and expression. CSCs harvested from the AutoCulture® system exhibited similar surface expression profiles and overall viability to those cultured manually.

Analysis of array comparative genomic hybridization (aCGH) and microarray

To detect genomic DNA mutations on AutoCulture®, we performed aCGH analysis (Agilent technologies) on day 7 and day 14 and compared them with the tissue derived from human right atrial appendage (RAA) (Figure 4A). There were no differences in genomic DNA mutation between CSCs in AutoCulture® and RAA. To investigate the global gene expression profile changes between CSCs in manual culture and CSCs in AutoCulture®, we performed a pairwise comparison of gene expression microarray data using NIA array analysis [18]. The results revealed a similar gene pattern between them (Figure 4B, Additional file 3). The "Symbol" of 162 gene probes was left blank in 258 overexpressed gene probes.

Discussion

Cell-based regenerative medicine is still in the early stages of development [19,20]. The quality of cells for transplant depends on the ability of skilled personnel to isolate, expand, and harvest cultured cells. For consistency of cell yield and phenotype, it is imperative that methodological consistency is strictly maintained. Automation greatly enhances the consistency of culture conditions and may thus reduce the variability in cell quality that is one of the great impediments to the widespread application of cell-based therapy till date. In this study, we used the automated cell culture system AutoCulture® to expand human CSCs isolated from the RAA for use in the ALCADIA clinical trial designed to assess the safety of cell-based therapy for patients with ischemic cardiomyopathy. RAA-derived cells containing CSCs exhibited similar growth rates and gene

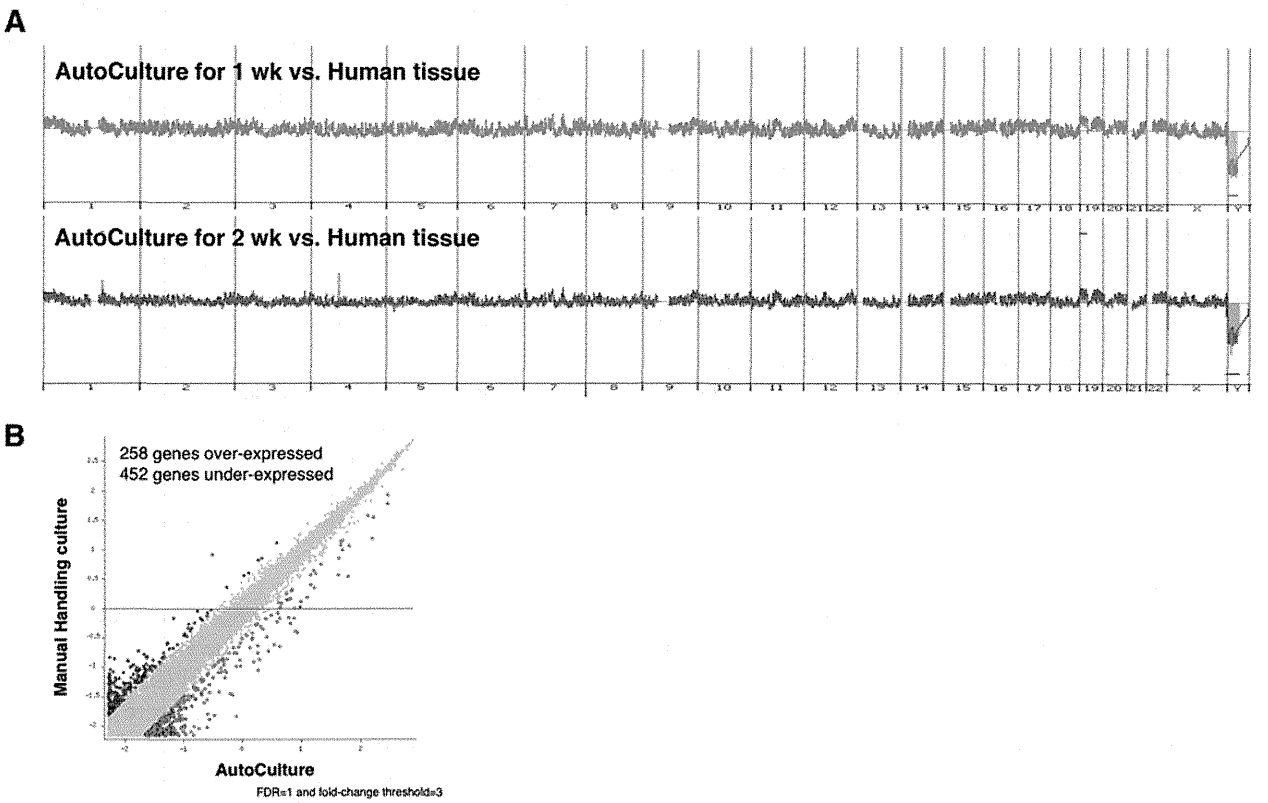

Figure 4 Global analysis of gene expression and genomic DNA mutations. (A) Comparison of array comparative genomic hybridization analysis. Human gDNA (from RAA) was compared to gDNA extracted from CSCs cultivated using AutoCulture® after 1 and 2 weeks using CGH arrays (arrays G4413A). **(B)** Microarray analysis of gene expression profiles. The pairwise scatter plot presents differences in gene expression on day 7 after seeding between manually cultured CSCs and those cultured using AutoCulture®. Grey dots represent transcripts with a subthreshold difference in expression. Red or green dots indicate those with at least a 3-fold difference in expression levels between the two groups. Gene expression levels are depicted on a log2 scale. The number of differentially expressed genes is indicated above.

expression profiles between manual and automated cultures. Thus, the AutoCulture® system effectively replicated manual culture and demonstrated scalability and stability in addition to safety and cost-effectiveness. Indeed, we found no significant differences in phenotype between the two culture methods. Cells in both the populations had similar morphologies, mean growth rates, and expression levels of genes associated with pluripotency and the mesenchymal lineage. In addition, the surface glycan profile was virtually identical, while aCGH analysis revealed no difference in genomic DNA mutation frequency. Finally, the approximately 41,000-probe Agilent Whole Human Genome Microarray chip G4112F showed that only approximately 1% of transcripts measured were significantly under- or overexpressed. The successful transfer of manual to automated cell culture may be attributable to the high flexibility of the machine, which can faithfully copy every step and condition, including media changes, splitting, and passaging in a controlled environment.

AutoCulture® is an all-in-one automated cell culture system consisting of robot arms, tube and flask decappers, flask holders, flask tappers, media pumps, a pipette head, a centrifugal separator, a rotating plate, and a CO_2 incubator. In addition to media change and passage, it permits routine observation. To automate these culture steps, it is necessary to program the humidity, temperature, volume and flow of liquid, and robot arm motion that transfers flasks from or into the CO_2 incubator or flask holder. Another automated cell culture platform, TAP CompacT, was also shown to be an effective system for culture of adherent cells by the Healthcare Engineering group [14]. However, the lack of a centrifugal separator in that system may result in differences between the manual and automated processes, possibly explaining why automation resulted in a smaller population of STRO-1+ cells and overall lower cell yield after the first passage [21]. STRO-1 expression is not a necessary or specific marker for stem or progenitor cells, and somatic stem cells may be more resistant to nutritional and chemical stress [22]. Residual trypsin in the culture media may have adversely affected the survival of differentiated cells, but it is not clear whether stem or progenitor cells can survive or not. On the other hand, the AutoCulture® system efficiently removes trypsin/EDTA by washing and centrifugation. There were no significant

differences in the surface marker expression profile or the mean rate of proliferation between these cells and those maintained manually, strongly suggesting that both populations of RAA-derived CSCs contain equal properties.

The AutoCulture® system can save labor and costs by expanding the scale of production and maintaining uniformity of results. In addition, this system can simultaneously cultivate different cells without cross-contamination because it can be equipped with a connecting hatch to multiple CO_2 incubators. Large-scale production and multi-sample cell culture capacity for cell transplantation may be a prerequisite for commercialization of cell products under current good manufacturing practice (cGMP) grade. Production methods for cell therapy should be designed to ensure that the end product is standardized and safe. cGMP is a quality assurance system that ensures that the cell product meets preset specifications with minimal lot-to-lot variability [23]. It requires traceability of raw materials used in cell culture and validated standard operating procedures (SOPs) throughout the process [24,25]. Current good tissue practice (cGTP) is intended to prevent human cells, tissues, and cellular and tissue-based products from contamination by infectious disease agents and to ensure that these cells and tissues maintain their integrity and function. The controlled environment of a carefully designed, constructed, validated, and maintained clean room will minimize the risks of environmental contamination and decrease the possibility of cross-contamination [26]. Based on cGMP, aseptic handling and filling of raw materials should be performed in a grade A environment (class 100) with a grade B background (class 1,000). Clean room disciplines, gowning procedures, cleaning programs, and maintenance of air handling units are included in SOPs. Environmental monitoring is essential in clean room quality control. Proper cleaning, maintenance, repair, and attire are major issues for cGMP [27].

Construction and maintenance of a cGMP facility is so expensive that it may be difficult to conform to these standards on a large scale without automation. Unlike manual culture, the robots enabled the environment in the cell culture cabinet to be completely separated from the external environment. Moreover, automated cell culture machines can be equipped with cleaning and monitoring systems to prevent contamination by microorganisms and cross-contamination by other cell types cultured in tandem. These properties may meet the stringent conditions for a human cell processing facility while reducing both construction and maintenance costs.

In Japan, the regulatory path of a regenerative cell therapy using this automated machine will be to obtain an approval for the end products, such as cells or tissues, based on the new guidelines and philosophy at an initial phase. An important requirement for obtaining approval is publication of the safety and reliability of the machine to produce the final biological products in a peer-reviewed journal. The similar properties of cell products between those obtained by machine and those obtained by manual culture, as demonstrated in this study, could support approval of a clinical trial using this machine, which is currently being planned.

Conclusion

AutoCulture® is one of the best candidates to solve the problems inherent in large-scale production and harvesting of human cells for clinical applications. The automated cell processing system can reproduce many complex operations performed by professional staff and can maintain multiple cell lines automatically. Thus, this automation system will be a powerful tool for both clinical trials exploring the potential of autologous or allogeneic cell-based regeneration therapies and for the commercialization.

Methods

Isolation of human CSCs containing atrial appendage

After this study was approved by the ethics committees of Tokyo Metropolitan Geriatric Hospital (ID: #220106), human cardiac tissue samples from RAA were surgically excised from 7 patients (60–75 years old) during cardiac surgery. All patients provided written informed consent. A cell population containing CSCs was acquired according to the current protocol for ALCADIA [28]. In brief, the tissue fragments were cut into 5 × 5-mm pieces and incubated with 0.2% collagenase type II and 0.1% DNase I (Worthington Biochemicals) at 37°C for 30 min. The cells were cultivated in a basic culture medium of Dulbecco's modified Eagle medium (DMEM)/F12 supplemented with 10% fetal bovine serum (FBS) and 40 ng/ml basic fibroblast growth factor (bFGF). The cells were seeded in 60-mm dishes coated with collagen type I. The cultured cells were passaged twice, harvested, and frozen until used in this experiment. P2 cell population was utilized as the starting material for this comparison experiment.

Cell expansion and harvesting

After thawing, the cells derived from the human atrium were seeded at 1×10^5 cells per 100-mm culture dish and cultivated for 5–7 days. The cells were split at 1:10 at 80%–90% confluence. The basic culture medium was replaced every 3 or 4 days. For automated culture, we used the same lot of CSCs. After seeding, the culture dishes were placed in the AutoCulture® chamber and transferred into the internal CO_2 incubator by the robot arm (Figure 1A, Additional file 4). For media replacement, the robot arm retrieved the culture dishes from the incubator and set them on a rotating table. The dish covers were removed by the robot arm, a specified amount of medium was discarded, fresh medium was supplied by a new pipette, the covers were returned,

and the culture dishes was transferred back to the CO_2 incubator. For passage, the old medium was removed and DPBS was pipetted onto the dishes under gentle shaking. After washing in DPBS, AutoCulture® supplied trypsin, oscillated the culture dishes, and returned them to the CO_2 incubator for a 5-min incubation. Following this, the robot arm moved the culture dishes onto the rotation table, added a prespecified volume of the basic culture media, and transferred the cell suspension from each dish to a separate 50-ml centrifuge tube. The cell suspension was centrifuged at 200 × *g* for 5 min at room temperature, and the supernatant was discarded. Fresh basic culture medium was supplied to the cell pellet, which was then resuspended. The washed cell suspension was subcultured at approximately 1:10 onto new culture dishes and returned to the CO_2 incubator.

Reverse transcription-polymerase chain reaction (RT-PCR)

Total RNA was extracted from cell populations containing CSCs, from human iPSCs, and raw human heart tissue samples using the RNeasy Plus Mini Kit (QIAGEN) as positive/negative control. Total RNA from human iPSCs and the human heart (Clontech Laboratories) was used as the positive control for each primer. Total RNA (500 ng per reaction) was converted to cDNA using the Transcriptor High Fidelity cDNA Synthesis Kit (Roche Applied Science) according to the manufacturer's protocol. Primers for the cardiac-specific transcription factors *NKX2.5* and *GATA4*; the stem cell markers *NANOG*, *OCT3/4*, *SOX2*, and *REX1*; and the housekeeping gene *GAPDH* were obtained from PrimerBank (Additional file 5).

Flow cytometric analysis

The cells (1×10^6 per reaction) were stained in autoMACS Running Buffer (Miltenyi Biotec.) with fluorescence-conjugated primary antibodies for 30 min at 4°C. The cells were then analyzed on the Attune Acoustic Focusing Cytometer (Applied Biosystem), and the data were analyzed using FlowJo 8.8.7 software (TOMY Digital Biology). Antibodies used for phenotyping included anti-human CD29-PE, CD90-PE, CD105-FITC, STRO-1-FITC, CD45-PE, and MHC class II-PE. Isotype controls were FITC-conjugated mouse IgG_1, PE-conjugated mouse IgG_1, and FITC-conjugated mouse IgM.

Lectin microarray analysis

Proteins were extracted from each cell population in hydrophobic and hydrophilic fractions using the CelLytic MEM Protein Extraction Kit (Sigma-Aldrich), as described previously [29]. Lectin microarray analysis was performed as described previously, with only minor modifications [30]. The glycoprotein (200 ng) was labeled with Cy3 monoreactive dye (GE Healthcare) in DPBS containing 0.5% Triton X-100 (PBSTx) at room temperature for 1 h. The Cy3-labeled glycoprotein solution (60 μl) was applied to the LecChip (GP Bioscience), which has triplicate spots specific for 45 lectins on each glass slide. An evanescent-field fluorescence scanner (GlycoStationTM Reader) was used to analyze the LecChip. All data were analyzed with GlycoStationTM Tools Signal Capture 1.0 and GlycoStationTM Tools Pro 1.0 software (GP Bioscience). To expand the dynamic range, the data were subjected to a gain-merging procedure, and the merged data were then normalized with max-normalization, as described previously [29].

aCGH analysis

Genomic DNA from the heart tissue and cultured cells was isolated using the DNeasy Blood & Tissue Kit (QIAGEN). Labeled test and reference DNAs were combined, denatured, preannealed with Cot-1 DNA (Invitrogen) and blocking agent, and then hybridized to the arrays (SurePrint G3 Human CGH Microarray 2x400K, Agilent Technologies). After hybridization and washing, the arrays were scanned at 3-μm resolution using an Agilent G2505C scanner. Images were analyzed with Feature Extraction software 10.7.3.1 (Agilent Technologies) using the CGH 107 Sep09 protocol for background subtraction and normalization.

Gene expression analysis

Gene expression analysis was performed using the Agilent Whole Human Genome Microarray chip G4112F (Agilent Technologies), which contains >41,000 probes. Raw data were normalized and analyzed by GeneSpring GX11 software (Silicon Genetics). Pairwise scatter plot analysis of the global gene expression profiles of both manually cultured cells and autocultured cells was performed on day 7 after thawing. The number of differentially expressed genes is indicated over each scatter plot. The NIA Array [18] web tool was used for pairwise scatter plot analysis. Gene expression microarray data have been submitted under accession number GSE 44032. Analysis of microarray experiments was conducted using the Aberration Detection Method-2 statistical algorithm (Agilent Technologies) on the basis of the combined log2 ratios at a threshold of 6.0. The data were centralized, and calls with average log2 ratios <0.3219 were filtered to exclude false positives.

Additional files

Additional file 1: Document 1. Specialization of the automated cell processing machine (Auto Culture®).

Additional file 2: Document 2. Quantitative cellular aspects for ALCADIA clinical trial.

Additional file 3: Table S1. Results of microarray analysis of CSCs in manual culture and AutoCulture®. To investigate the differences in global gene expression profile between CSCs in manual culture and CSCs in AutoCulture®, we performed a pairwise comparison of gene expression

microarray data using NIA array analysis. The results revealed similar gene expression patterns between them.

Additional file 4: Movie 1. AutoCulture®.Movie of the culture robot in AutoCulture®.

Additional file 5: Table S2. RT-PCR primer sequences. RT-PCR primer sequences were obtained from PrimerBank (http://pga.mgh.harvard.edu/primerbank/).

Abbreviation

CSC: Cardiac stem cells; FACS: Fluorescence-activated cell sorting; MSCs: Mesenchymal stem cells; aCGH: Array comparative genomic hybridization; RAA: Right atrial appendage; cGMP: Current good manufacturing practice; SOPs: Standard operating procedures; cGTP: Current good tissue practice; bFGF: Basic fibroblast growth factor.

Competing interests

DK, MYI, KM, TK, YI, MT, AU and SG declare that they have no competing interests. KW and TS are employees of Kawasaki Heavy Industries, Ltd.

Authors' contributions

DK, MT, AU, and SG designed the research; DK, KW, YI, KM, MYI, and performed the experiments; DK, MT, and SG analyzed the data; and DK, TK, YI, and SG wrote the manuscript. All authors read and approved the final manuscript.

Acknowledgments

We would like to express our sincere thanks to Nakata M. (Kyoto Prefectural University of Medicine) and Akutsu H (National Center for Child Health and Development). This research was supported by grants from Ministry of Education, Culture Sports, Science and Technology (MEXT) of Japan.

Author details

[1]Department of Regenerative Medicine, Kyoto Prefectural University of Medicine, 465 Kajii-cho, Kawaramachi-Hirokoji, Kamigyo-ku, Kyoto 602-8566, Japan. [2]System Technology Development Center, Kawasaki Heavy Industries, Ltd., 3-1-1 Higashi Kawasaki-cho, Chuo-ku, Kobe 650-8670, Japan. [3]Department of Reproductive Biology and Pathology, National Center for Child Health and Development, 2-10-1 Okura, Setagaya-ku, Tokyo 157-8535, Japan. [4]Department of Cardiovascular Medicine, Kyoto Prefectural University of Medicine, 465 Kajii-cho, Kawaramachi-Hirokoji, Kamigyo-ku, Kyoto 602-8566, Japan. [5]Department of Vascular Medicine, Tokyo Metropolitan Institute of Gerontology, 35-2 Sakae-cho, Itabashi-ku, Tokyo 173-0015, Japan.

Received: 7 May 2013 Accepted: 12 November 2013
Published: 15 November 2013

References

1. Takehara N, Tsutsumi Y, Tateishi K, Ogata T, Tanaka H, Ueyama T, Takahashi T, Takamatsu T, Fukushima M, Komeda M, *et al*: **Controlled delivery of basic fibroblast growth factor promotes human cardiosphere-derived cell engraftment to enhance cardiac repair for chronic myocardial infarction.** *J Am Coll Cardiol* 2008, **52**(23):1858–1865.
2. Smith RR, Barile L, Cho HC, Leppo MK, Hare JM, Messina E, Giacomello A, Abraham MR, Marban E: **Regenerative potential of cardiosphere-derived cells expanded from percutaneous endomyocardial biopsy specimens.** *Circulation* 2007, **115**(7):896–908.
3. Rota M, Padin-Iruegas ME, Misao Y, De Angelis A, Maestroni S, Ferreira-Martins J, Fiumana E, Rastaldo R, Arcarese ML, Mitchell TS, *et al*: **Local activation or implantation of cardiac progenitor cells rescues scarred infarcted myocardium improving cardiac function.** *Circ Res* 2008, **103**(1):107–116.
4. Vogel G: **Stem cells for sale.** *Science* 2010, **330**(6008):1173.
5. Tran CA, Burton L, Russom D, Wagner JR, Jensen MC, Forman SJ, DiGiusto DL: **Manufacturing of large numbers of patient-specific T cells for adoptive immunotherapy: an approach to improving product safety, composition, and production capacity.** *J Immunother* 2007, **30**(6):644–654.
6. Soncin S, Lo Cicero V, Astori G, Soldati G, Gola M, Surder D, Moccetti T: **A practical approach for the validation of sterility, endotoxin and potency testing of bone marrow mononucleated cells used in cardiac regeneration in compliance with good manufacturing practice.** *J Transl Med* 2009, **7**:78.
7. Joannides A, Fiore-Heriche C, Westmore K, Caldwell M, Compston A, Allen N, Chandran S: **Automated mechanical passaging: a novel and efficient method for human embryonic stem cell expansion.** *Stem Cells* 2006, **24**(2):230–235.
8. Kino-Oka M, Ogawa N, Umegaki R, Taya M: **Bioreactor design for successive culture of anchorage-dependent cells operated in an automated manner.** *Tissue Eng* 2005, **11**(3–4):535–545.
9. Terstegge S, Laufenberg I, Pochert J, Schenk S, Itskovitz-Eldor J, Endl E, Brustle O: **Automated maintenance of embryonic stem cell cultures.** *Biotechnol Bioeng* 2007, **96**(1):195–201.
10. Thomas RJ, Anderson D, Chandra A, Smith NM, Young LE, Williams D, Denning C: **Automated, scalable culture of human embryonic stem cells in feeder-free conditions.** *Biotechnol Bioeng* 2009, **102**(6):1636–1644.
11. Koike H, Kubota K, Sekine K, Takebe T, Ouchi R, Zheng YW, Ueno Y, Tanigawa N, Taniguchi H: **Establishment of automated culture system for murine induced pluripotent stem cells.** *BMC Biotechnol* 2012, **12**:81.
12. Thomas RJ, Chandra A, Liu Y, Hourd PC, Conway PP, Williams DJ: **Manufacture of a human mesenchymal stem cell population using an automated cell culture platform.** *Cytotechnology* 2007, **55**(1):31–39.
13. Hubbell JA, Palsson BO, Papoutsakis ET: **Preface: tissue engineering and cell therapies: II.** *Biotechnol Bioeng* 1994, **43**(8):683.
14. Thomas R, Chandra A, Hourd P, Williams D: **Cell culture automation and quality engineering: a necessary partnership to develop optimized manufacturing processes for cell-based therapies.** *J Assoc Lab Autom* 2008, **13**(3):152–158.
15. Thomas RJ, Hourd PC, Williams DJ: **Application of process quality engineering techniques to improve the understanding of the in vitro processing of stem cells for therapeutic use.** *J Biotechnol* 2008, **136**(3–4):148–155.
16. Takehara N, Ogata T, Nakata M, Kami D, Nakamura T, Matoba S, Gojo S, Sawada T, Yaku H, Matsubara H: *The ALCADIA (Autologous Human Cardiac-Derived Stem Cell to Treat Ischemic Cardiomyopathy) trial*, Circulation. PHILADELPHIA, PA: LIPPINCOTT WILLIAMS & WILKINS 530 WALNUT ST; 2012:19106–3621. USA: 2783–2783.
17. Toyoda M, Yamazaki-Inoue M, Itakura Y, Kuno A, Ogawa T, Yamada M, Akutsu H, Takahashi Y, Kanzaki S, Narimatsu H, *et al*: **Lectin microarray analysis of pluripotent and multipotent stem cells.** *Genes Cells* 2011, **16**(1):1–11.
18. Sharov AA, Dudekula DB, Ko MS: **A web-based tool for principal component and significance analysis of microarray data.** *Bioinformatics* 2005, **21**(10):2548–2549.
19. Ptaszek LM, Mansour M, Ruskin JN, Chien KR: **Towards regenerative therapy for cardiac disease.** *Lancet* 2012, **379**(9819):933–942.
20. Gojo S, Toyoda M, Umezawa A: **Tissue engineering and cell-based therapy toward integrated strategy with artificial organs.** *J Artif Organs* 2011, **14**(3):171–177.
21. Liu Y, Hourd P, Chandra A, Williams DJ: **Human cell culture process capability: a comparison of manual and automated production.** *J Tissue Eng Regen Med* 2010, **4**(1):45–54.
22. Kuroda Y, Kitada M, Wakao S, Nishikawa K, Tanimura Y, Makinoshima H, Goda M, Akashi H, Inutsuka A, Niwa A, *et al*: **Unique multipotent cells in adult human mesenchymal cell populations.** *Proc Natl Acad Sci USA* 2010, **107**(19):8639–8643.
23. Unger C, Skottman H, Blomberg P, Dilber MS, Hovatta O: **Good manufacturing practice and clinical-grade human embryonic stem cell lines.** *Human Mol Genet* 2008, **17**(R1):R48–R53.
24. Allport-Settle MJ: *Good Manufacturing Practice (GMP) Guidelines*. Raleigh: Pharmalogika; 2009.
25. Burger SR: **Current regulatory issues in cell and tissue therapy.** *Cytotherapy* 2003, **5**(4):289–298.
26. USP: *32-NF 27 Cell and gene therapy products*. United States Pharmacopeia, Rockville: Manufacturing of cell therapy products; 2008.
27. Niazi SK: *Sterile products, vol. 6*. London: Informa Healthcare Inc; 2009.
28. Takehara NOT, Nakata M, Kami D, Matoba NT, Gojo S, Sawada T, Yaku H, Matsubara H: *The ALCADIA (autologous Human Cardiac-derived Stem Cell To Treat Ischemic Cardiomyopathy) Trial*, Late Breaking Clinical Trial Application. Los Angeles: American Heart Association, Scientific Session; 2012.
29. Kuno A, Itakura Y, Toyoda M, Takahashi Y, Yamada M, Umezawa A, Hirabayashi J: **Development of a data-mining system for differential**

profiling of cell glycoproteins based on lectin microarray. *J Proteom Bioinfo* 2008, 1(2):5.

30. Itakura Y, Kimura M, Gojo S, Toyoda M, Kami D, Motomura N, Umezawa A, Kyo S, Ono M: **Glycan profiling using a lectin microarray is a novel validation tool for monitoring the damage to freeze-thawed cells.** *Low Temp Med* 2011, **37**:7.

doi:10.1186/1472-6750-13-102
Cite this article as: Kami *et al.*: Large-scale cell production of stem cells for clinical application using the automated cell processing machine. *BMC Biotechnology* 2013 **13**:102.

MCB
Journals.ASM.org

Noncanonical NOTCH Signaling Limits Self-Renewal of Human Epithelial and Induced Pluripotent Stem Cells through ROCK Activation

Takashi Yugawa,[a] Koichiro Nishino,[b] Shin-ichi Ohno,[a] Tomomi Nakahara,[a] Masatoshi Fujita,[c] Naoki Goshima,[d] Akihiro Umezawa,[e] Tohru Kiyono[a]

Division of Virology, National Cancer Center Research Institute, Tokyo, Japan[a]; Laboratory of Veterinary Biochemistry and Molecular Biology, Faculty of Agriculture, University of Miyazaki, Miyazaki, Japan[b]; Department of Cellular Biochemistry, Graduate School of Pharmaceutical Sciences, Kyushu University, Fukuoka, Japan[c]; Molecular Profiling Research Center for Drug Discovery, National Institute of Advanced Industrial Science and Technology, Tokyo, Japan[d]; Department of Reproductive Biology, National Center for Child Health and Development, Tokyo, Japan[e]

NOTCH plays essential roles in cell fate specification during embryonic development and in adult tissue maintenance. In keratinocytes, it is a key inducer of differentiation. ROCK, an effector of the small GTPase Rho, is also implicated in keratinocyte differentiation, and its inhibition efficiently potentiates immortalization of human keratinocytes and greatly improves survival of dissociated human pluripotent stem cells. However, the molecular basis for ROCK activation is not fully established in these contexts. Here we provide evidence that intracellular forms of NOTCH1 trigger the immediate activation of ROCK1 independent of its transcriptional activity, promoting differentiation and resulting in decreased clonogenicity of normal human keratinocytes. Knockdown of NOTCH1 abrogated ROCK1 activation and conferred sustained clonogenicity upon differentiation stimuli. Treatment with a ROCK inhibitor, Y-27632, or ROCK1 silencing substantially rescued the growth defect induced by activated NOTCH1. Furthermore, we revealed that impaired self-renewal of human induced pluripotent stem cells upon dissociation is, at least in part, attributable to NOTCH-dependent ROCK activation. Thus, the present study unveils a novel NOTCH-ROCK pathway critical for cellular differentiation and loss of self-renewal capacity in a subset of immature cells.

Notch is an evolutionarily conserved cell surface receptor that plays essential roles in cell fate decisions as well as maintenance of self-renewing tissue organization (1–3). Notch proteins are expressed in most adult tissues, and the biological consequence of Notch activation is critically dependent on the cell type and the cellular context (4–7). In keratinocytes, Notch1 has been shown to be a key inducer of differentiation (8–11). Keratinocyte-specific conditional deletion of the *Notch1* gene results in epidermal hyperproliferation and tumor formation in mice, thus indicating a tumor-suppressive role of Notch1 in mammalian postnatal epidermis (12). The Notch receptor is generally activated by interaction with its ligands displayed on the neighboring cell surface. Cell-cell contact is a strong inducer of keratinocyte differentiation in culture, where Notch1 acts as a critical determinant in the transition from proliferation to differentiation (13, 14). Due to *cis* inhibition of Notch by its ligand when these are expressed on the same cell surface (15, 16), the relative increase in expression levels of the Notch receptor over its ligand is also shown to be a pivotal cue to activate Notch signaling and generate distinct cell fates among neighboring cells (17). We previously demonstrated that p53 and TAp63 transactivate *Notch1* gene expression and induce keratinocyte differentiation, while ΔNp63 is a transcriptional repressor of the *Notch1* gene and inhibits keratinocyte differentiation (14, 18). p63, especially ΔNp63α, is a master regulator of development and maintenance of stratified epithelia (19, 20). ΔNp63α expresses predominantly in the basal proliferating compartment, where Notch1 signaling is suppressed (21). In suprabasal layers, downregulation of ΔNp63α by miR-203 or another factor(s) (22–24) evokes activation of Notch1 signaling, which in turn further downmodulates ΔNp63α expression so as to induce differentiation (9, 21). The Notch1 precursor (~300 kDa) is processed by furin protease in the Golgi apparatus and transported to the cell surface as a mature heterodimeric complex (~120/~180 kDa) that is held by Ca^{2+}-dependent noncovalent interaction (25). Ligand binding dissociates the Notch1 extracellular domain (~180 kDa) by *trans* endocytosis. The residual transmembrane domain (~120 kDa) is sequentially cleaved by tumor necrosis factor alpha-converting enzyme/metalloprotease (TACE) and γ-secretase, resulting in release of the Notch1 intracellular domain (~110 kDa) into the cytosol (3). EDTA is reported to activate Notch signaling through disruption of the heterodimeric complex of Notch1 (25) and thus used as a tool to study Notch1 signaling (26–28). In canonical Notch1 signaling, the liberated Notch1 intracellular domain (~110 kDa) translocates into the nucleus to activate Notch-responsive genes, such as Hes1, by making a complex with CSL family members {CBF1 and RBP-Jκ in mammals, Suppressor of hairless [Su(H)] in *Drosophila*, and Lag1 in *Caenorhabditis elegans*} and its transcriptional coactivator Mastermind (MAM). Besides this canonical pathway, accumulating evidence suggests noncanonical cytoplasmic Notch functions (29–31).

Received 11 May 2013 Returned for modification 5 June 2013
Accepted 20 August 2013
Published ahead of print 9 September 2013
Address correspondence to Tohru Kiyono, tkiyono@ncc.go.jp.
Supplemental material for this article may be found at http://dx.doi.org/10.1128/MCB.00577-13.

doi:10.1128/MCB.00577-13

Rho-associated coiled-coil protein kinases (ROCKs) (also known as Rho kinases [ROKs]) are effectors of the small GTPase Rho and belong to a family of protein serine/threonine kinases (32–34). Activated ROCK proteins regulate actomyosin cytoskeletal dynamics and contractility through phosphorylation of multiple downstream targets, such as myosin phosphatase (MYPT1), to drive cell motility. In keratinocytes, ROCK proteins play a role in differentiation (35, 36), and their selective inhibitor, Y-27632, completely inhibits differentiation as well as stratification of keratinocytes in organotypic raft culture (37). Y-27632 also enables efficient immortalization of not only human primary keratinocytes but also several other primary human epithelial cells in the presence of fibroblast feeders (37, 38), although molecular details supporting immortalization remain elusive.

In addition, Y-27632 has been shown to increase the survival rate and cloning efficiency of human embryonic stem cells (hESCs) dissociated with EDTA (39) through blocking the Rho-ROCK-myosin light chain signaling cascade (40, 41). However, the precise mechanisms by which EDTA activates ROCK have not been elucidated (41, 42).

These results let us hypothesize a possible link between NOTCH1 and ROCK activation. Here we show a novel function of NOTCH1 as a critical upstream regulator of ROCK1 and its relevance to loss of self-renewal capacity in human keratinocytes as well as human induced pluripotent stem (hiPS) cells.

MATERIALS AND METHODS

Cell culture. Normal human cervical keratinocytes (HCKs) were obtained with written consent from a patient who underwent abdominal surgery for a gynecological disease other than cervical cancer and were retrovirally transduced with the catalytic subunit of human telomerase reverse transcriptase (hTERT) for immortalization (HCK1Ts) (14). HCK1Ts were cultured in serum-free keratinocyte-SF medium supplemented with 5 ng/ml epidermal growth factor (EGF) and 50 μg/ml of bovine pituitary extract (Invitrogen, Life Technologies, Saint Aubin, France). Primary human dermal keratinocytes (HDKs) were purchased from Cell Applications Inc. (San Diego, CA). Primary human foreskin keratinocytes (HFKs) were obtained from Denise A. Galloway (Fred Hutchinson Cancer Research Center, Seattle, WA). HDKs and HFKs were cultured in serum-free keratinocyte-SF medium supplemented with 5 ng/ml EGF and 50 μg/ml of bovine pituitary extract (Invitrogen, Life Technologies). Human endometrium cells were collected by scraping tissues from surgical specimens, with signed informed consent and with ethical approval of the Institutional Review Board of the National Institute for Child Health and Development, Japan. All experiments involving human cells and tissues were performed in line with Tenets of the Declaration of Helsinki. Human iPS cell lines, MRC-hiPSCs and UtE-hiPSCs, were established from MRC-5 fetal lung fibroblasts (43) and UtE1104 endometrium-derived cells (44), respectively, via procedures described by Takahashi et al. (45) with slight modification (46, 47). Human iPS cells were maintained in iPSellon medium (Cardio Incorporated, Osaka, Japan) supplemented with 10 ng/ml recombinant human basic fibroblast growth factor (bFGF) (Wako Pure Chemical Industries, Ltd., Osaka, Japan) in the presence of irradiated mouse embryonic fibroblast (MEF) feeders.

Retroviral vector construction and transduction. Retroviral vector plasmids were constructed using the Gateway system according to the manufacturer's instructions (Invitrogen). Segments of the intracellular domain of human NOTCH1 (ICN1), a truncated form of MAML1 corresponding to amino acids 13 to 74 fused to N-terminal hemagglutinin (HA) tag (MAML61-3HA), and c-MYC were cloned and recombined into retroviral expression vectors to generate pCLXSN-ICN1 (14), pCLXSN-MAML61-3HA (48, 49), and pCMSCVpuro-c-MYC (50). Human ROCK1, ROCK1ΔC241, ROCK1-D1113A, ROCK1-K105A, ICN1-ERT, ICN2-ERT2, RhoA, and enhanced green fluorescent protein (EGFP) were cloned into a lentiviral vector, CSII-TRE-Tight-RfA, in which the elongation factor promoter in CSII-EF-RfA (a gift from Hiroyuki Miyoshi, RIKEN, BioResource Center) was replaced with the tetracycline-responsive promoter from pTRE-Tight (Clontech, Mountain View, CA). The Notch1 short hairpin RNA (shRNA) vectors were described previously (14, 18). To generate ROCK1- or ROCK2-specific shRNA expression vectors pCL-SI-MSCVpuro-ROCK1Ri-1,-2,-3 and pCL-SI-MSCVpuro-ROCK2Ri-1,-2,-3, the following sequences were chosen as the targeted sites: 5′-GTACTTGTATGAAGATGA-3′ (51), 5′-GGTATATGCTATGAAGCTT-3′, and 5′-GCGAAATGGTGTAGAAGAA-3′ for ROCK1 and 5′-GAAACTAATAGGACACTAAC-3′ (52), 5′-GGTTTATGCTATGAAGCTT-3′, and 5′-GGATAAACATGGACATCTA-3′ for ROCK2. The retroviral vector and packaging constructs pCL-GagPol and pEF6/env (10A1) or the lentiviral vector and packaging constructs pCAG-HIVgp and pCMV-VSV-G-RSV-Rev were cotransfected into 293FT cells (Invitrogen) using TransIT-293 (Mirus Co., Madison, WI) according to the manufacturer's instructions, and the culture fluid was harvested at 60 to 72 h posttransfection. Titers of the recombinant viruses were determined by drug resistance with HeLa cells or a real-time PCR method (TaKaRa, Otsu, Japan) to detect the viral RNA genome, yielding titers equivalent to greater than 1×10^6 CFU/ml. Following addition of the recombinant viral fluid to cells in the presence of 4 μg/ml Polybrene, infected cells were selected in the presence of 0.5 μg/ml puromycin or 50 μg/ml G418, and promptly after drug selection, pooled cell populations were used for most subsequent experiments.

Tet-On keratinocytes. HCK1T cells were stably transduced with Tet-On ADV and tTS expression vectors, encoding the rtTA-Advanced transactivator and transcriptional silencer, respectively (Clontech). The resultant HCK1T Tet-On cells were then introduced with CSII-TRE-Tight-ROCK1, ROCK1ΔC241, ROCK1-D1113A, ROCK1-K105A, ICN1-ERT, ICN2-ERT2, RhoA (constitutive active and dominant negative forms), and EGFP by retroviral gene transfer. Induction of these transgenes was routinely achieved by treatment with 1 μg/ml doxycycline (DOX) for 72 h.

Inhibitors. The following pharmacological inhibitors were used: cycloheximide (CHX) (239764; Calbiochem, Darmstadt, Germany), z-VAD-fmk (caspase inhibitor IV) (219007; Calbiochem), γ-secretase inhibitor IX (DAPT) (565784; Calbiochem), Y-27632 (08945-84; Nacalai Tesque, Kyoto, Japan), C3 ADP-ribosyltransferase (Rho inhibitor) (CT04; Cytoskeleton, Inc., Denver, CO), and blebbistatin (sc-203532; Santa Cruz Biotechnology, Santa Cruz, CA). Cells were pretreated with inhibitors for 2.5 h. For DAPT, in addition to pretreatment, cells were incubated with this inhibitor during and after exposure to EDTA or differentiation stimuli for up to 48 h.

Induction of keratinocyte differentiation. At 48 h after plating, HCK1T cells were treated with 2.5 mM EDTA in phosphate-buffered saline without Ca^{2+} and Mg^{2+} [PBS(−)] for 10 min or exposed to 0.7% and 5% bovine serum albumin (BSA) or 10% serum-containing medium in the presence of 10 μg/ml of bovine pituitary extract. To induce ligand-dependent NOTCH activation, HCK1T cells were harvested in subconfluent and 7-day-postconfluent states. HCK1T cells were also introduced with ICN1 by retroviral gene transfer to induce differentiation.

Dissociation of human iPS cells. First, hiPSC colonies were treated with collagenase IV solution at 37°C for 10 min. The detached hiPSC clumps were recovered, incubated with 0.005% trypsin–2.5 mM EDTA solution at 37°C for 5 min, and dissociated into single cells by pipetting. The dissociated cells were counted with Vi-CELL (Beckman Coulter, Brea, CA) and seeded onto MEF feeders.

Immunoblotting. Whole-cell protein extracts were used for analysis, and immunoblotting was conducted as described previously (14). Primary antibodies against Notch1 (sc-6014; Santa Cruz Biotechnology), activated Notch1 (cleaved Notch1 Val1744 2421; Cell Signaling Technology, Danvers, MA), Notch2 (clone C651.6DbHN; Developmental Studies Hybridoma Bank, University of Iowa), Hes1 (Toray Industries, Inc., To-

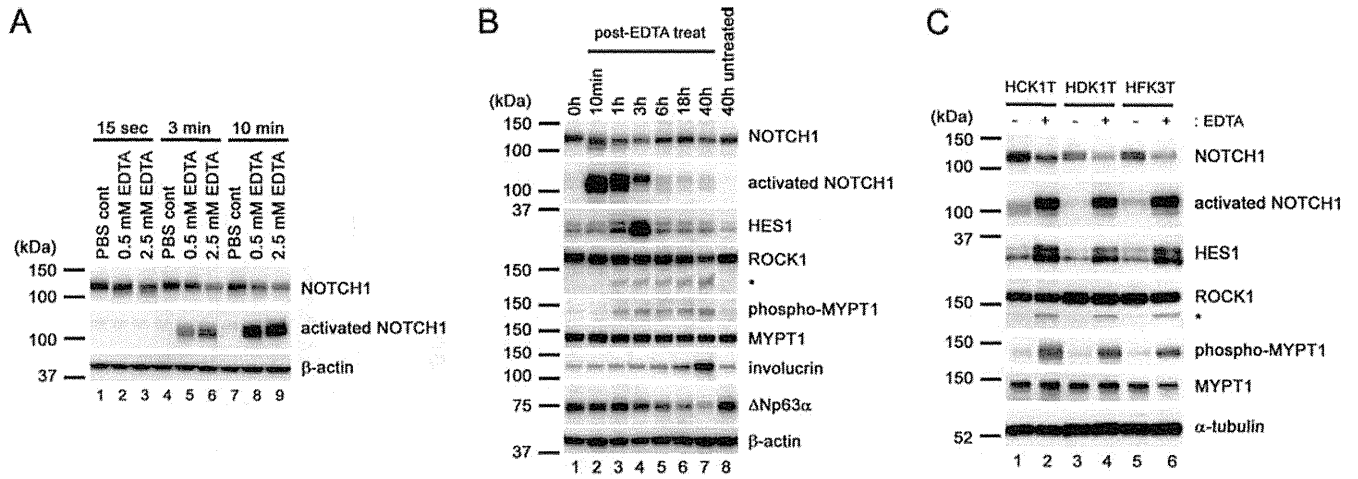

FIG 1 Immediate activation of ROCK1 following release of the NOTCH1 intracellular fragment in normal human keratinocytes. (A) HCK1T cells were either left untreated (PBS cont) or treated with 0.5 or 2.5 mM EDTA in PBS(−) for indicated time points. Cell lysates were prepared and analyzed by immunoblotting with the indicated antibodies. (B) HCK1T cells were either left untreated or treated with 2.5 mM EDTA in PBS(−) for 10 min at 37°C. After washing twice with PBS(−), cells were incubated with keratinocyte-SF medium. Cell lysates were prepared at the indicated time points after EDTA treatment. Extracts were analyzed by immunoblotting with the indicated antibodies. The band corresponding to the furin-processed transmembrane domain of NOTCH1 with a molecular mass of 120 kDa is shown as NOTCH1 here. An asterisk indicates a smaller fragment of ROCK1 protein with a molecular mass of ~130 kDa. (C) Keratinocytes from cervix (HCK1T), dermis (HDK1T), and foreskin (HFK1T) were either left untreated or treated with 2.5 mM EDTA for 10 min. After washing twice with PBS(−), cells were incubated with keratinocyte-SF medium for 3 h. Extracts were analyzed by immunoblotting with the indicated antibodies.

kyo, Japan), Hey1 (sc-16424; Santa Cruz Biotechnology), involucrin (clone SY5; Sigma, Saint-Quentin Fallavier, France), loricrin (AF 62; Covance, Princeton, NJ), Rock1 (sc-5560; Santa Cruz Biotechnology), phospho-MYPT1 (07-251; Merck-Millipore, Billerica, MA), MYPT1 (07-672; Merck-Millipore), Rock2 (sc-5561; Santa Cruz Biotechnology), p63 (clone 4A4; Santa Cruz Biotechnology), caspase-3 (9662; Cell Signaling Technology), poly(ADP-ribose) polymerase (PARP) (9542; Cell Signaling Technology), OCT3/4 (sc-5279; Santa Cruz Biotechnology), HA tag

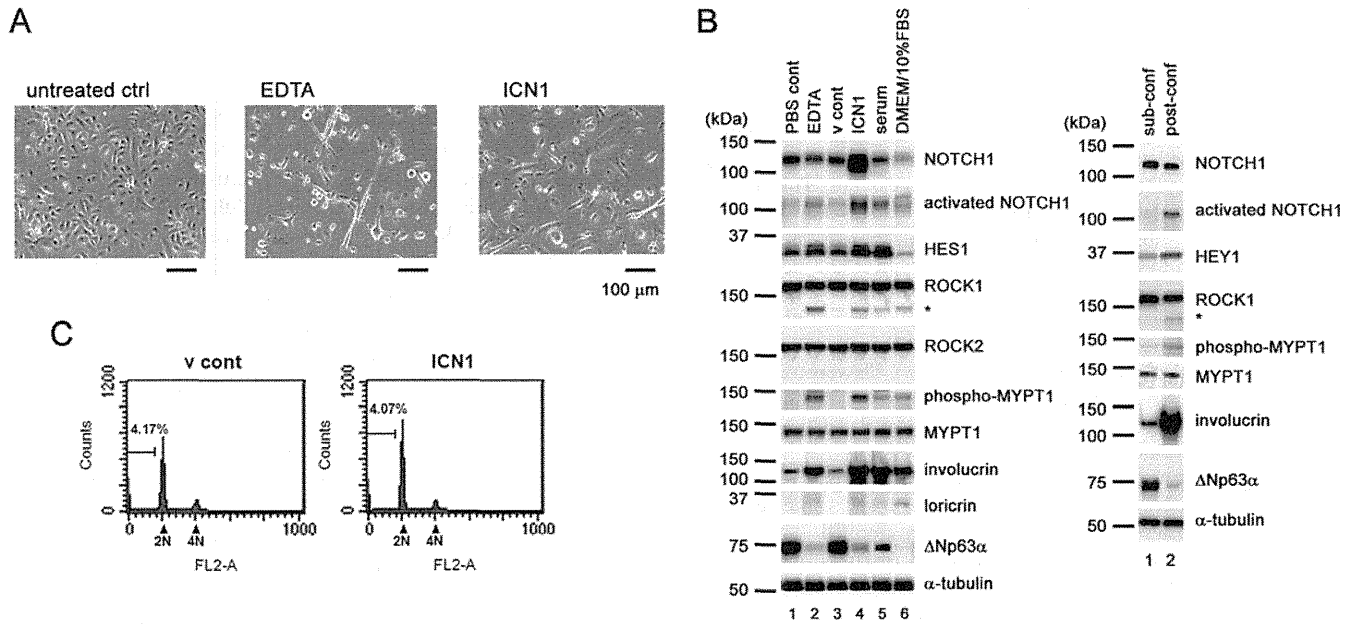

FIG 2 Expression of the NOTCH1 intracellular domain, serum exposure, and cell-cell contact cause ROCK activation and cellular differentiation in normal keratinocytes. (A) HCK1T cells were either left untreated or treated with 2.5 mM EDTA and incubated with keratinocyte-SF medium after treatment. HCK1T cells were transduced with the constitutively active form of NOTCH1 (ICN1). Typical areas were photographed at 3 days posttreatment or posttransduction. Scale bars represent 100 μm. (B) HCK1T cells were either left untreated or treated with 2.5 mM EDTA and incubated with keratinocyte-SF medium after treatment. HCK1T cells were transduced with the constitutively active form of NOTCH1 (ICN1) or control (v cont). HCK1T cells were exposed to serum-containing keratinocyte-SF medium (serum) or Dulbecco modified Eagle medium with 10% fetal bovine serum (DMEM–10% FBS). Cell lysates were harvested at 3 days posttreatment or posttransduction. HCK1T cells were also harvested in subconfluent and 7-day-postconfluent states. Extracts were analyzed by immunoblotting with the indicated antibodies. (C) HCK1T cells were transduced with the constitutively active form of NOTCH1 (ICN1) or control (v cont). At 3 days posttransduction, cells were collected and DNA content was analyzed by flow cytometry. The percentage of apoptotic cells displaying a sub-G_1 DNA content is shown between markers.

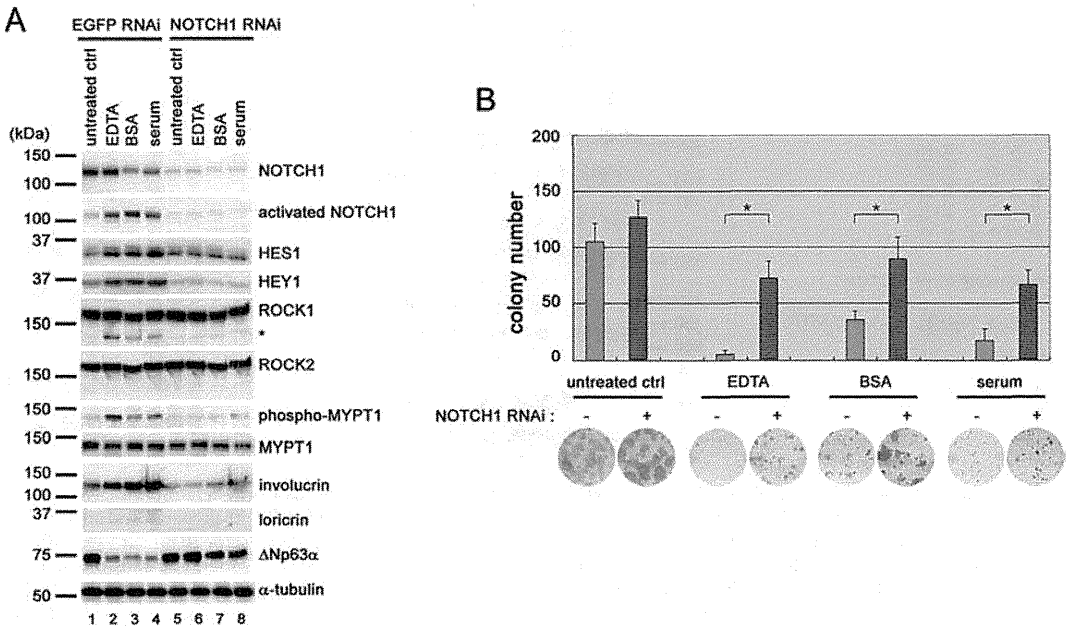

FIG 3 Knockdown of NOTCH1 abrogates the production of the smaller ROCK1 and MYPT1 phosphorylation with restoration of clonogenic growth potential in normal keratinocytes exposed to EDTA, BSA, or serum. (A) HCK1T cells stably expressing NOTCH1 shRNA (NOTCH1 RNAi) or control shRNA (EGFP RNAi) were treated with 2.5 mM EDTA, 5% bovine serum albumin, or 10% serum or left untreated. Cells were harvested at 3 days posttreatment, and cell extracts were subjected to immunoblotting analysis with the indicated antibodies. (B) Aliquots of 500 HCK1T cells stably expressing NOTCH1 shRNA (NOTCH1 RNAi) or control shRNA (EGFP RNAi) were seeded on 35-mm dishes under sparse conditions. Then cells were treated similarly to those for panel A. After being cultivated for 2 weeks, the cells were stained with Giemsa's dye, and colonies were counted. The photographs are of representative dishes, and the graph represents means ± SDs. *, $P < 0.05$ according to Student's t tests.

(ab72479; Abcam, Paris, France), β-actin (sc-1616; Santa Cruz Biotechnology), α-tubulin (2144; Cell Signaling Technology), and GAPDH (glyceraldehyde-3-phosphate dehydrogenase) (AM4300; Ambion, Inc., Austin, TX) were used as probes. Horseradish peroxidase-conjugated anti-mouse and anti-rabbit (Jackson ImmunoResearch Laboratories, West Grove, PA) and anti-goat (sc-2033; Santa Cruz Biotechnology) immunoglobulins were used as the secondary antibodies. The LAS3000 charge-coupled device (CCD) imaging system (Fujifilm Co. Ltd., Tokyo, Japan) was employed for detection of proteins visualized by Lumi-light Plus Western blotting substrate (Roche, Basel, Switzerland). The exposure time was adjusted to keep the signals within a linear and nonsaturated range, and the band signal intensities were quantified by densitometry using imaging software (Fujifilm Multi-Gauge) after normalization to that of internal controls, such as β-actin, α-tubulin, or GAPDH.

Fluorescence-activated cell sorting analysis. Cells were treated with a CycleTEST Plus DNA reagent kit (Becton Dickinson, Franklin Lakes, NJ) for propidium iodide staining and then analyzed with a Becton Dickinson FACSCalibur instrument.

Clonogenic assay. Aliquots of 500 cells were seeded on 35-mm dishes under sparse conditions. After cultivation for 2 weeks, the cells were stained with Giemsa's dye, and the colonies were counted.

Statistical analysis. Statistical analysis was carried out using Microsoft Excel software. Unless stated otherwise, all data are presented as means ± standard deviations (SD) from at least three independent experiments; error bars represent SD in all figures. Intergroup comparisons were performed by the two-tailed Student's t test. A P value of <0.05 was considered to be statistically significant.

RESULTS

Immediate activation of ROCK following expression of the NOTCH intracellular form. Previous work has shown stabilization of the noncovalent interaction between a ligand-binding extracellular domain and a transmembrane signaling subunit of NOTCH by millimolar Ca^{2+} and transient activation of this heterodimeric NOTCH receptor by EDTA-mediated shedding of its extracellular domain, independent of cell-cell contact or binding of a ligand displayed on the surface of a neighboring cell (25). In line with this notion, somatic activating mutations of NOTCH1 within the heterodimerization domain are frequently found in human T cell acute lymphoblastic leukemia and are thought to increase the production of the intracellular form of NOTCH1 (53). To ascertain whether calcium depletion could induce activation of NOTCH1, normal human keratinocytes, which were maintained with serum-free, low-calcium medium, were subjected to EDTA treatment. We found that this chelator treatment elicited immediate and robust expression of the cleaved intracellular form of NOTCH1 in a time- and dose-dependent manner (Fig. 1A). Time course experiments revealed that this intracellular NOTCH1 arose transiently and that thereafter activation of the NOTCH target gene was induced, as well as upregulation of a differentiation marker and downregulation of a keratinocyte stemness marker, ΔNp63α, in agreement with its proposed role in keratinocyte differentiation (Fig. 1B) (8, 9, 11). We also noted that the EDTA-treated cells underwent a drastic morphological change (Fig. 2A) with increased motility (see Movie S1 in the supplemental material), which was also seen in cells transduced with the NOTCH1 intracellular domain (ICN1) in much the same fashion (Fig. 2A). We have previously shown that these morphologically altered cells are differentiating cells strongly expressing K10 and involucrin (14).

ROCK inhibition with Y-27632 has been reported to inhibit differentiation and increase the proliferative capacity of primary human keratinocytes in culture, pointing to a role for ROCK

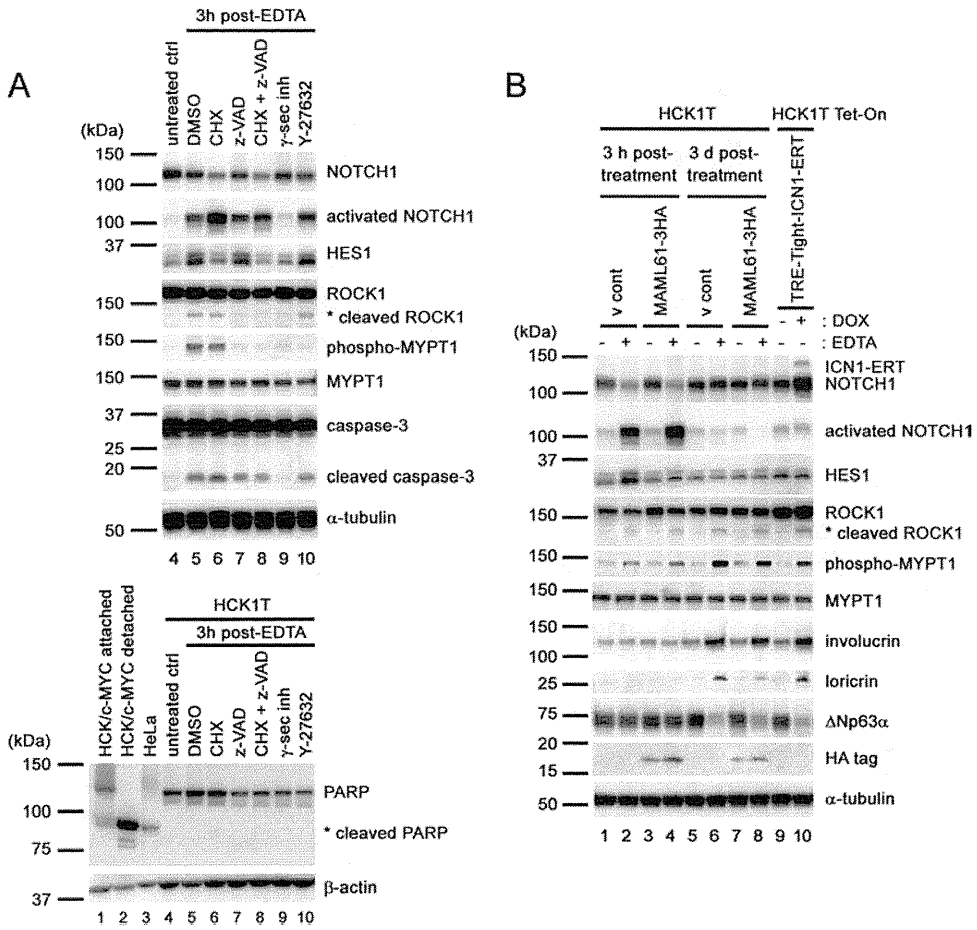

FIG 4 ROCK1 activation is independent of NOTCH1 transcriptional activity. (A) HCK1T cells, pretreated where indicated with 10 μg/ml cycloheximide (CHX) for 2.5 h, 20 μM z-VAD-fmk for 2.5 h, 10 μM γ-secretase inhibitor (DAPT) for 2.5 h, or 10 μM Y-27632 for 2.5 h, were either left untreated or treated with 2.5 mM EDTA for 10 min and incubated with keratinocyte-SF medium for 3 h. Whole-cell extracts were subjected to immunoblotting analysis with the indicated antibodies. As a positive control for PARP cleavage, cell extracts from detached HCKs after c-MYC transduction were used. (B) HCK1T cells were stably transduced with dominant negative MAML1 (MAML61-3HA) or vector control (v cont). Cells were exposed to 2.5 mM EDTA (+) or left untreated (−), and cell lysates were prepared at 3 h and 72 h posttreatment. HCK1T Tet-On cells were then introduced with the TRE-Tight-ICN1-ERT tetracycline-inducible gene cassette. HCK1T Tet-On-ICN1-ERT cells were either left untreated (−) or treated (+) with 1 μg/ml doxycycline (DOX) for 72 h.

in keratinocyte differentiation (35, 37). These observations prompted us to determine whether NOTCH activation by EDTA treatment during passage could induce differentiation or a decrease in proliferative potential, possibly through ROCK activation. As shown in Fig. 1B, immediately after production of the NOTCH1 intracellular form, additional ROCK1 polypeptides of smaller size emerged. The ROCK1 fragment with a relative molecular weight of ~130,000 was reminiscent of that observed in cells undergoing apoptosis, which has been identified as a caspase-3-cleaved, constitutively activated form (54, 55). Indeed, MYPT1, a downstream molecule of ROCK, was phosphorylated concomitantly with the appearance of the smaller ROCK1 proteins, indicating increased ROCK1 activity in cells with active NOTCH1 signaling.

In keratinocytes, NOTCH1 has been shown to be activated in response to differentiation stimuli such as suspension in methylcellulose, confluence-triggered cell-cell contact, and serum exposure, as well as with genotoxic stress (13, 14, 18, 49, 56). Therefore, we examined whether differentiation stimuli or expression of ICN1 could cause ROCK activation. The additional smaller proteins of ROCK1, but not ROCK2, and phosphorylation of MYPT1 were observed in response to serum exposure (Fig. 2B, left panel). Since albumin is the major protein in serum, to which approximately half of extracellular calcium is bound, we further tested the possibility that albumin exerts a differentiation-inducing effect through a mechanism similar to that for EDTA. As expected, albumin exposure also induced activation of NOTCH1, production of the smaller ROCK1, and upregulation of the differentiation markers (Fig. 3A, lane 3). Similarly, retroviral transduction of keratinocytes with ICN1 gave rise to the smaller ROCK1 in association with MYPT1 phosphorylation (Fig. 2B, left panel). Of importance, confluence-triggered cell-cell contact also induced smaller ROCK1 and MYPT1 phosphorylation, indicating that the ligand-mediated NOTCH activation is responsible for these events (Fig. 2B, right panel). Assuming that activated NOTCH1 evokes some apoptotic cascade, ROCK activation may occur in parallel in cells undergoing apoptosis. However, we failed to detect any indication of apoptotic cell death after ICN1 transduction (Fig. 2C). To further corroborate involvement of NOTCH1 in ROCK1 activation, we knocked down NOTCH1 expression. In contrast to the control case, NOTCH1 silencing abrogated the production of the smaller

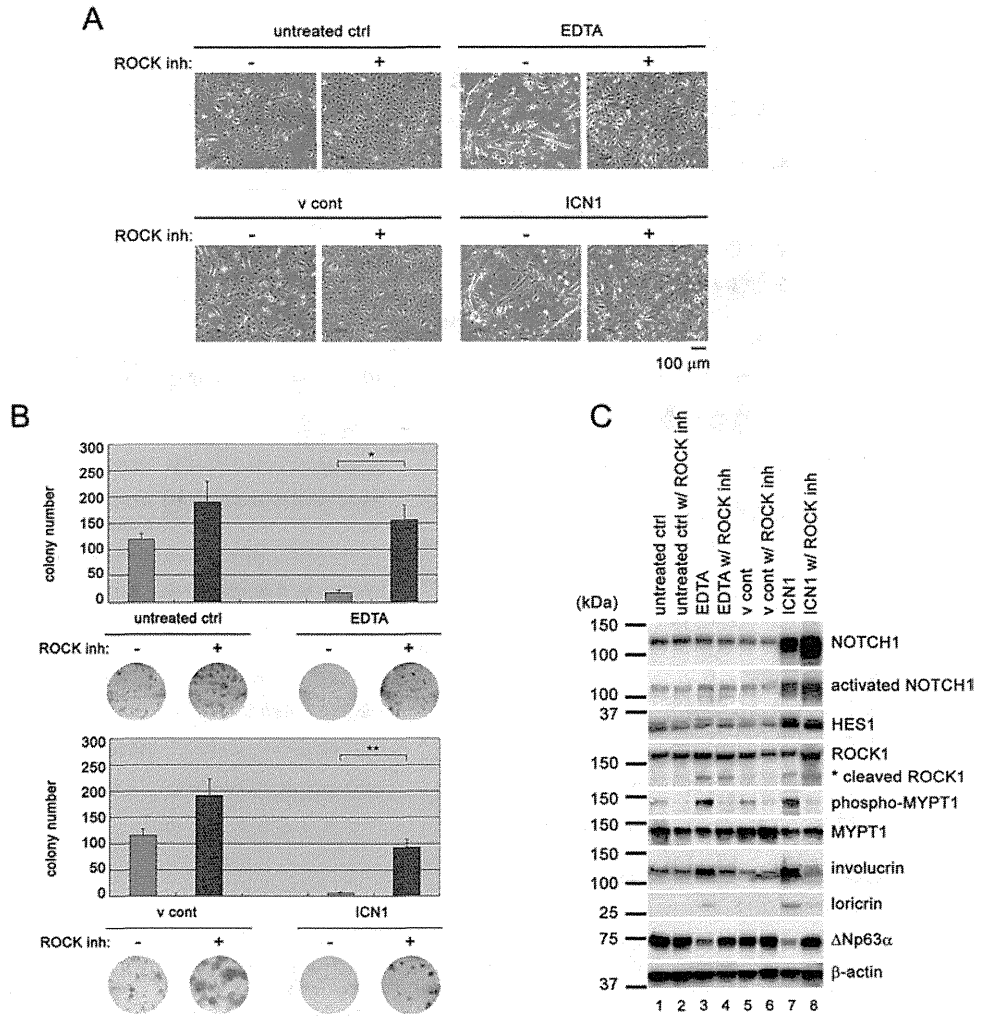

FIG 5 ROCK inhibition alleviates the growth-suppressive and differentiation-inducing effects of NOTCH1. (A) HCK1T cells pretreated with or without Y-27632 were either left untreated, treated with 2.5 mM EDTA, or transduced with ICN1 or vector control (v cont). Thereafter, cells were incubated in the presence or absence of Y-27632. Typical areas were photographed at 72 h after EDTA treatment. (B) Aliquots of 500 HCK1T cells were seeded on 35-mm dishes under sparse conditions. Cells pretreated with or without Y-27632 were then either left untreated, treated with 2.5 mM EDTA for 10 min, or transduced with ICN1 or vector control (v cont). After being cultivated for 2 weeks, the cells were stained with Giemsa's dye, and colonies were counted. The photographs are of representative dishes, and the graph represents means ± SDs. *, $P < 0.05$; **, $P < 0.01$ (according to Student's *t* tests). (C) Cells were treated similarly to those for panel A and incubated for 72 h. Cell extracts were subjected to immunoblotting analysis with the indicated antibodies.

ROCK1 and MYPT1 phosphorylation after differentiation stimuli (Fig. 3A) with restoration of clonogenic growth potential (Fig. 3B). Treatment with a γ-secretase inhibitor had the same effects as NOTCH1 knockdown (Fig. 4A and unpublished observations). These results suggest that the observed ROCK activation is not an outcome of apoptosis but is positively regulated by NOTCH1 signaling in differentiating cells.

The intracellular form of NOTCH is responsible for ROCK activation independently of its transcriptional activity. Given the immediate appearance of the smaller ROCK1 after expression of the intracellular NOTCH1, it can be hypothesized that NOTCH1 activation of ROCK1 does not occur through *de novo* protein expression. In an effort to clarify this, we treated cells with cycloheximide (CHX), an inhibitor of translation. While CHX treatment completely inhibited induction of the NOTCH1 transcriptional target, HES1, it did not affect the generation of the smaller ROCK1 and MYPT1 phosphorylation (Fig. 4A, upper panel, compare lanes 5 and 6). Since NOTCH1 requires the transcriptional coactivator, MAML1, in its transactivation complex, we also assessed the effect of dominant negative MAML1, MAML61-3HA. While exogenous expression of MAML61-3HA blocked the induction of HES1, it exerted no effect on the smaller ROCK1 production, MYPT1 phosphorylation, and expression of a differentiation marker, involucrin (Fig. 4B). It is still possible that the canonical NOTCH1 signaling plays a role in differentiation at a later stage, as the level of a terminal differentiation marker, loricrin, appeared to be attenuated to some extent in MAML61-3HA-expressing cells. To further explore the transcription-independent function of NOTCH1 in ROCK1 activation, we established tetracycline-inducible ICN1-ERT keratinocytes, expressing a chimeric protein consisting of the intracellular domain of NOTCH1 fused at the amino terminus to a mutated ligand-binding domain of the estrogen receptor (ERT) (57). In the presence of doxycycline (DOX) for 3 days and without addition of the

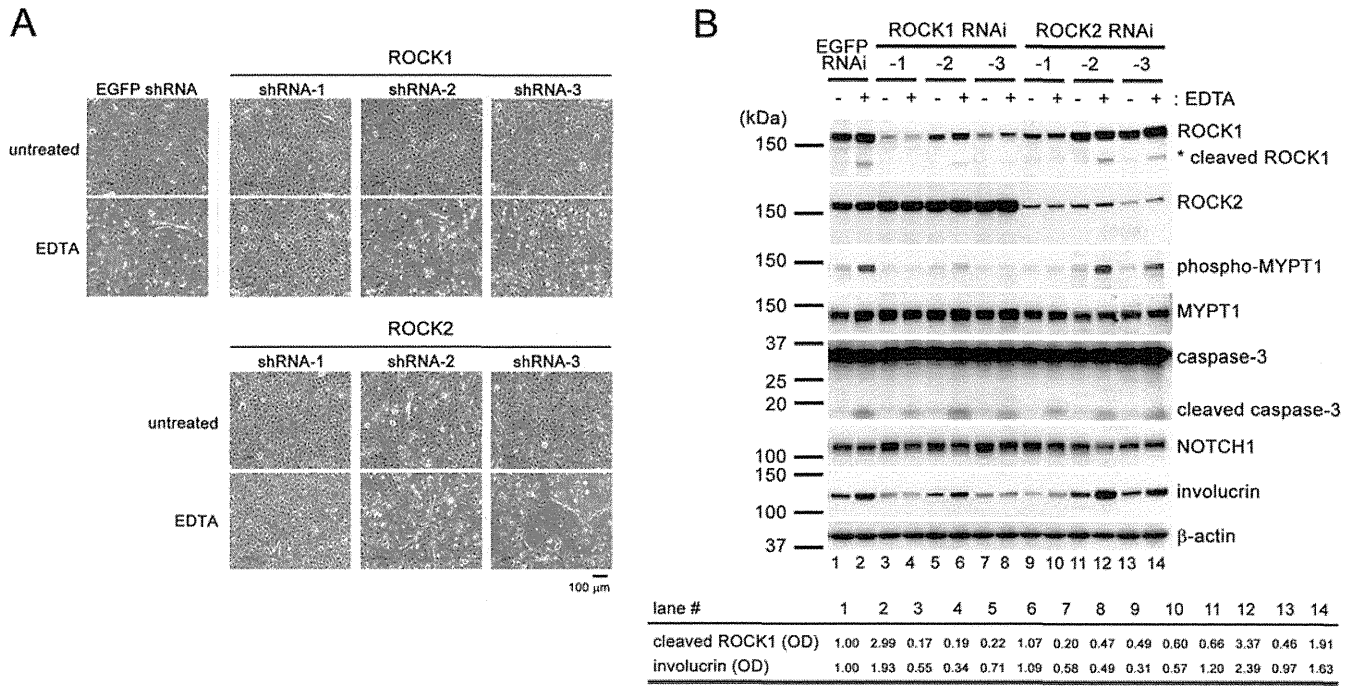

FIG 6 *Knockdown of ROCK1 inhibits keratinocyte differentiation after EDTA treatment.* (A) HCK1T cells stably transduced with shRNAs for ROCK1 and -2 were either left untreated or treated with 2.5 mM EDTA and then incubated with keratinocyte-SF medium. Typical areas were photographed at 3 days after EDTA treatment. Note that ROCK2 shRNA-2 knocked down ROCK1 expression as well. (B) HCK1T cells were transduced with three different shRNAs for ROCK1 and -2 or with control shRNA for EGFP. Cells were then either left untreated (−) or treated (+) with 2.5 mM EDTA for 10 min. After cultivation for 72 h, cells were harvested and analyzed by immunoblotting. The band optical densities (OD) for the cleaved ROCK1 and involucrin were quantified densitometrically, normalized to that of β-actin with the value for untreated control defined as 1.

estrogen homolog, ICN1-ERT did not transactivate the target gene but triggered the smaller ROCK1 production and MYPT1 phosphorylation (Fig. 4B, compare lanes 9 and 10). These results indicate a transcription-independent or cytoplasmic function of NOTCH1 in control of ROCK1 activity and its roles in cellular differentiation.

To elucidate whether the additional smaller fragment of ROCK1 is a constitutively active form generated by caspase-3-mediated cleavage (54, 55), cells were treated with the caspase inhibitor z-VAD prior to EDTA exposure. In the presence of active forms of NOTCH1, z-VAD markedly blocked generation of the smaller ROCK1 as well as MYPT1 phosphorylation (Fig. 4A, upper panel, compare lanes 5 and 7), indicating that the NOTCH intracellular form could induce immediate and constitutive activation of ROCK1 through caspase. This activation of caspase is much weaker than that observed in apoptotic cells, since cleavage of the well-known caspase substrate PARP was marginally detected only when pretreated with CHX (Fig. 4A lower panel), suggesting a nonapoptotic function of caspase activation in keratinocyte differentiation.

ROCK inhibition rescues the phenotype induced by NOTCH activation. Next, to address whether ROCK activation is the critical downstream event in NOTCH signaling, we tested whether the NOTCH gain-of-function phenotype could be reversed by ROCK inhibition. To this end, we assessed the differentiation status and clonogenic growth potential after EDTA treatment or ICN1 transduction in the presence of a ROCK inhibitor. ROCK inhibition significantly restored the morphology and clonogenicity of keratinocytes upon EDTA treatment or ICN1 transduction (Fig. 5A and B), and suppressed both induction of differentiation markers and reduction of ΔNp63α (Fig. 5C). Silencing of ROCK1 but not ROCK2 also blocked differentiation after EDTA treatment (Fig. 6A and B). Intriguingly, continuous ROCK inhibition rendered cells permissive to constitutive ICN1 expression as well as HES1 induction without indication of differentiation and maintained growth potential during at least three passages, while only cells expressing a small amount of ICN1 survived without the ROCK inhibitor (Fig. 7A). ROCK inhibition may allow increased NOTCH1 levels, possibly due to counterbalancing its biological effects. ROCK inhibitor withdrawal resulted in a prompt resumption of differentiation following MYPT1 phosphorylation in ICN1-expressing cells (Fig. 7B). These results suggest that ROCK is the critical downstream effector of NOTCH signaling in loss of stemness and differentiation of keratinocytes.

Ectopic expression of constitutively active ROCK1 induces keratinocyte differentiation. We next asked whether activated ROCK1 itself could initiate differentiation of normal human keratinocytes. For this purpose, we established several lines of keratinocytes expressing various exogenous ROCK1 mutants in a doxycycline-dependent manner. Upon induced expression of ROCK1ΔC241, a truncated mutant corresponding to a caspase-cleaved constitutively active form, downregulation of ΔNp63α and upregulation of a differentiation marker were evident to a level comparable to that observed in ICN1-ERT cells (Fig. 8A, compare lanes 2 and 8). Expression of wild-type ROCK1 exhibited only marginal effects (Fig. 8A, lane 6), while caspase-cleavage resistant ROCK1-D1113A and kinase-inactive ROCK1-K105A mutants failed to induce differentiation (Fig. 8A, lanes 10 and 12).